MR Imaging of Normal Epiphyseal Development and Common Epiphyseal Disorders[1]

Camilo Jaimes, MD
Nancy A. Chauvin, MD
Jorge Delgado, MD
Diego Jaramillo, MD, MPH

Abbreviations: ADC = apparent diffusion coefficient, DDH = developmental dysplasia of the hip, DEH = dysplasia epiphysealis hemimelica, GAG = glycosaminoglycan, GRE = gradient-recalled echo, JOCD = juvenile osteochondritis dissecans, LCP = Legg-Calvé-Perthes, SOC = secondary ossification center, STIR = short inversion time inversion-recovery, ZPC = zone of provisional calcification

RadioGraphics 2014; 34:449–471

Published online 10.1148/rg.342135070

Content Codes: MK MR PD

[1]From the Department of Radiology, Children's Hospital of Philadelphia, 34th Street and Civic Center Boulevard, Philadelphia, PA 19104-4399 (C.J., N.A.C., J.D., D.J.); and Perelman School of Medicine at the University of Pennsylvania, Philadelphia, Pa (N.A.C., D.J.). Presented as an education exhibit at the 2012 RSNA Annual Meeting. Received April 19, 2013; revision requested June 11 and received August 5; accepted August 8. For this journal-based SA-CME activity, the authors, editor, and reviewers have no financial relationships to disclose. **Address correspondence to** N.A.C. (e-mail: *chauvinn@email.chop.edu*).

ONLINE-ONLY SA-CME LEARNING OBJECTIVES

After completing this journal-based SA-CME activity, participants will be able to:

- Describe the normal development of the epiphysis and recognize normal variants at MR imaging.
- Discuss the role of MR imaging in assessment of congenital and developmental conditions that affect unossified epiphyses.
- Identify and describe common pathologic conditions that affect the epiphysis, including fractures, infection, trauma, and avascular necrosis.

See www.rsna.org/education/search/RG.

TEACHING POINTS

See last page

During infancy and childhood, multiple developmental changes occur in the epiphysis. Initially the epiphysis is composed entirely of hyaline cartilage. As skeletal maturation progresses, one or several secondary ossification centers (SOCs) develop within the epiphyseal cartilage. The SOCs enlarge by endochondral ossification and undergo marrow transformation in a process analogous to that of the primary physis and metaphysis. Magnetic resonance (MR) imaging can be used to evaluate vascularity, marrow, and cartilage and plays a critical role in the assessment of epiphyseal disorders in children. In cases of shoulder and hip dysplasia, MR imaging demonstrates unossified structures and helps guide treatment. In cases of trauma, the intracartilaginous pathway of fractures, the degree of physeal involvement, and early bridge formation can be assessed. With the use of intravenous gadolinium-based contrast material, avascular necrosis and reperfusion can be characterized. This article reviews the normal structure of the epiphysis, its appearance at MR imaging, and age-related changes to the epiphysis. Common conditions that lead to epiphyseal damage in children are reviewed, with an emphasis on the role of MR imaging in diagnosis, prognosis, and treatment.

Introduction

Epiphyseal disorders are an important source of morbidity in children. During infancy and childhood, the skeleton grows rapidly and is very vulnerable. Injury to the developing epiphyseal cartilage and secondary ossification center (SOC) can lead to early joint degeneration and lifelong sequelae. The chondro-osseous transitions at the epiphyses constitute weak links that often are injured during periods of active growth such as puberty and adolescence. Magnetic resonance (MR) imaging plays a crucial role in the assessment of epiphyseal disorders by demonstrating cartilaginous and osseous structures in great detail without the use of ionizing radiation. With the aid of intravenous gadolinium-based contrast material and new sequences such as diffusion-weighted imaging, MR imaging can be used to provide further insights into tissue perfusion, composition, and microstructure.

The epiphysis develops as a mass of hyaline cartilage at the articulating end of a bone. As skeletal maturation progresses, one or several SOCs develop within the epiphyseal cartilage. MR imaging can demonstrate developmental changes in the epiphysis, such as ossification and marrow transformation, that should not be confused with disease (1). The types of pathologic conditions that affect the epiphysis are determined in part by the degree of skeletal maturation. Changes in vascularity, marrow, and cartilage influence the manifestation of epiphyseal abnormalities, which include developmental disorders, infection, avascular necrosis, and tumors.

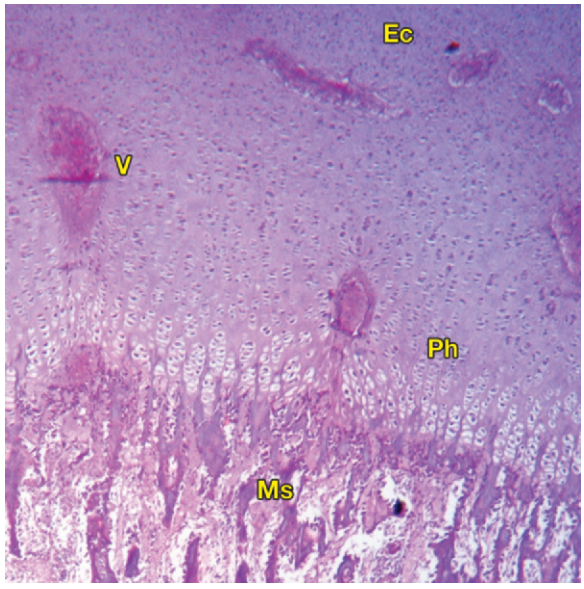

Figure 1. Normal histologic appearance of the epiphysis in the phalanx of a child. Photomicrograph (original magnification, ×40; hematoxylin-eosin stain) shows the epiphyseal cartilage (*Ec*), which contains numerous chondrocytes in an amorphous matrix. Vessels (*V*) are seen as they course through the cartilage. Columns of chondrocytes seen in the physis *(Ph)* are continuous with the metaphyseal spongiosa (*Ms*).

This article reviews the normal structure of the epiphysis, its MR imaging appearance, and age-related structural changes. Common conditions that lead to epiphyseal damage in children are reviewed, with emphasis on the role of MR imaging in diagnosis, prognosis, and treatment.

Normal Epiphysis

Structure and Histology

At birth, the immature epiphysis contains three types of hyaline cartilage: articular, epiphyseal, and physeal (2). The epiphyseal cartilage is located in the core of the epiphysis and is more abundant during the fetal and neonatal periods. It contains numerous chondrocytes scattered in a matrix rich in collagen (types II, IX, X, and XI), glycosaminoglycans (GAGs), and other noncollagenous proteins (2). The matrix also contains abundant water that is tightly bound to the proteins (2). Vessels course through a series of specialized vascular canals (Fig 1) (3). The cartilage in the center of the epiphysis undergoes changes before epiphyseal ossification. Vascular canals coalesce into a discrete network and release metalloproteinases (gelatinase B and collagenase-3) that result in the breakdown of the cartilaginous matrix (4). The chondrocytes also undergo hypertrophic changes before ossification. The cellular and matrix changes form what has been termed the *pre-ossification center*, which becomes mineralized to form the SOC. The ossification center is originally spherical but becomes hemispherical as it comes into closer contact with the metaphysis.

The articular cartilage is located in the outermost layer of the epiphysis and persists even after skeletal maturity. Its matrix contains aggrecan, type II collagen, and up to 70% water by volume (5). In contrast to the epiphyseal cartilage, the articular cartilage is completely avascular and contains very few cells (less than 2% by volume). Electron microscopy has been used to describe five zones in the articular cartilage (listed from outer to inner): the lamina splendens and the superficial, transitional, radial, and calcified layers. In the outer layers, collagen has a tangential arrangement that parallels the articular surface, whereas in the inner layers, it assumes a radial orientation (6).

The third type of hyaline cartilage is physeal cartilage, which is highly cellular (up to 75% by volume) (7). This subspecialized type of hyaline cartilage is responsible for the synthesis of new bone from cartilage, a process known as endochondral ossification. The primary physis is a thin disk located between the epiphyseal cartilage and metaphysis that is responsible for longitudinal bone growth (8). Chondrocytes in the physis are arranged in distinct columns parallel to the long axis of the bone. The chondrocytes originate in the germinal layer, which is located on the epiphyseal aspect of the physis. As they advance toward the metaphysis, the chondrocytes proliferate, hypertrophy, and finally undergo apoptosis as mineralization of the matrix occurs in the zone of provisional calcification (ZPC) (2). The SOC also enlarges by endochondral ossification from a spherical or secondary physis analogous to the primary physis (2). The germinal layer of the secondary physis is in the external aspect of the developing SOC, and the columns are arranged radially. As in the development of the SOC, the secondary physis is initially spherical but becomes hemispherical as it attenuates in the area adjacent to the physis and metaphysis. The

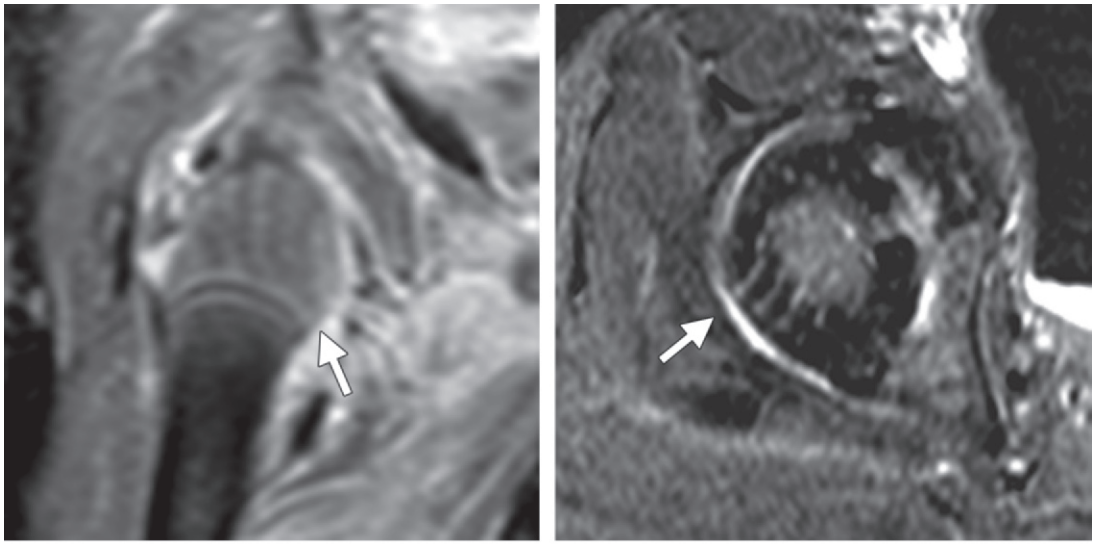

a. b.

Figure 2. Normal enhancement of the epiphyseal vessels. **(a)** Coronal postcontrast T1-weighted MR image of the hip in a 2-month-old girl shows parallel vessels with no SOC (arrow). **(b)** Axial postcontrast MR subtraction image of the hip in a 6-month-old boy demonstrates a radial arrangement of vessels (arrow) and a central enhancing SOC.

newly synthesized bone is at the periphery of the SOC and hence is analogous to the juxtaphyseal metaphysis.

Vascularity

Two separate vascular beds in the metaphysis and epiphysis are responsible for perfusion of the ends of the bone. The metaphysis has a rich vascular supply derived from the nutrient and metaphyseal arteries (8). The metaphyseal vessels reach the spongiosa and loop before the ZPC (8). The main function of these vessels is to trigger apoptosis of the chondrocytes in the lower hypertrophic zone and deliver the substrates necessary for mineralization. Disruption of the metaphyseal vascular supply results in the extension of unmineralized cartilage into the metaphysis (9). The abundant vascularity and slow flow in the capillary bed renders metaphyses vulnerable to blood-borne diseases such as infection and metastasis (3,10).

In the epiphysis, the vessels do not form a capillary bed but instead course through a series of canals in the cartilage that contain arterioles, venules, sinusoidal capillaries, loose connective tissue, and undifferentiated mesenchymal cells (3). These canals are responsible for nutrition and removal of waste products from the epiphyseal and physeal cartilage and the SOC. Cartilage canals also play a critical role in the development of the SOC by triggering breakdown of the cartilaginous matrix, providing substrates for mineralization, and facilitating invasion of osteogenic precursors (4). Initially the canals are nonanastomosing and parallel, but after the development of the SOC, the canals in the cartilage become oriented radially around the center (Fig 2) (1,3). Perfusion to the epiphysis is scanty and fragile, which predisposes young patients to avascular necrosis (11).

Teaching Point

During infancy, normal transphyseal vessels serve as anastomoses between the epiphyseal and metaphyseal vascular beds. Fenestrations on the physis increase the epiphyseal vascular supply but allow pathologic conditions such as infection to spread. Transphyseal anastomoses decrease with age and completely disappear at approximately 18 months of age (10).

MR Imaging

The signal intensity characteristics of cartilage at conventional MR imaging reflect mainly the amount of water within the matrix and cells and its degree of binding to macromolecules. On T1-weighted MR images, all hyaline cartilage has intermediate signal intensity, and the ZPC demonstrates very low signal intensity (Fig 3). On high-spatial-resolution fluid-sensitive MR images such as T2-weighted and short inversion time inversion-recovery (STIR) images, articular cartilage shows high signal intensity and epiphyseal cartilage shows very low signal intensity because of the strong binding of water to macromolecules. On these images, the primary physis demonstrates a trilaminar appearance, with high signal intensity in the resting and hypertrophic zones, low signal intensity in the ZPC, and high signal intensity in the metaphyseal spongiosa (Fig 4)

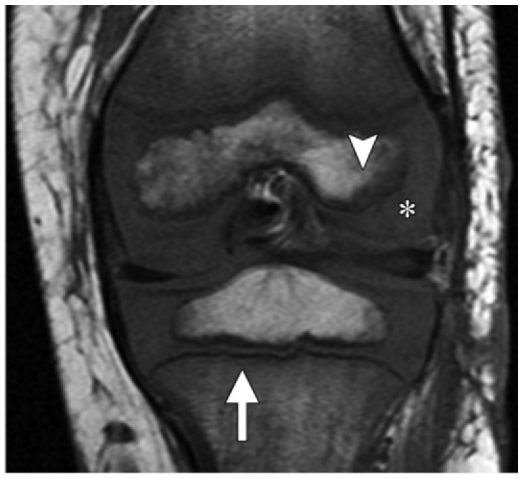

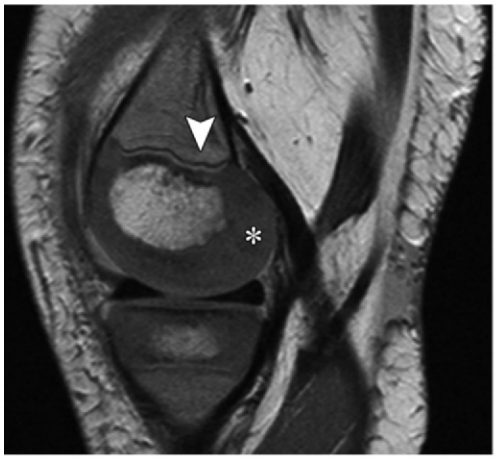

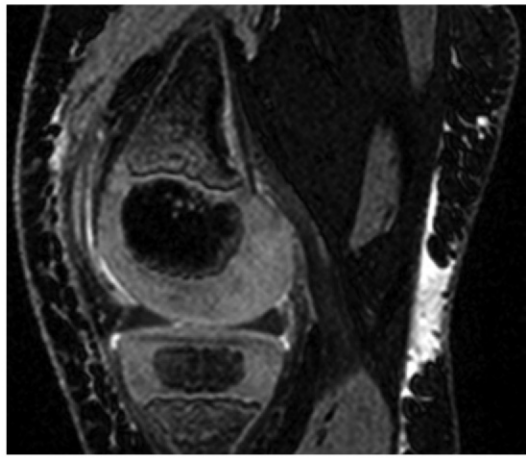

Figure 3. Normal cartilage in the knee of a 4-year-old boy. **(a)** Coronal T1-weighted MR image shows intermediate signal intensity in the epiphyseal cartilage (*). The ZPC has low signal intensity (arrow), and the periphery of the SOC contains hematopoietic marrow (arrowhead) **(b)** Sagittal intermediate-weighted MR image shows intermediate signal intensity in the epiphyseal cartilage (*) and high signal intensity in the physis (arrowhead). **(c)** Sagittal gradient-recalled echo (GRE) MR image shows high signal intensity in all forms of cartilage and very low signal intensity in the bone.

Figure 4. Zonal distinction of the epiphysis and physis. On a sagittal fat-saturated T2-weighted MR image of the knee in a 7-year-old boy, the primary physis (bracket) demonstrates a trilaminar appearance (high-low-high signal intensity) at the physis, ZPC, and metaphyseal spongiosa more superiorly. The SOC is surrounded by the secondary physis (arrow).

(2). The secondary physis demonstrates similar signal intensity characteristics (2). On GRE MR images, all cartilage demonstrates high signal intensity, while bone demonstrates very low signal intensity because of increased susceptibility from mineralized trabeculae (12).

MR imaging provides valuable insight into the different stages of ossification. Before the appearance of the SOC, the increase in free water and increased cellular volume lead to T2 prolongation that can be appreciated as high-signal-intensity foci on T2-weighted images (13). At MR imaging, preossification changes have been identified in the trochlea of the humerus and in the posterior femoral condyles (Fig 5) (13,14). However, these changes are ubiquitous at other sites with active endochondral ossification. In children aged 6–8 years, normal ossification of the femoral condyles can have a misleading appearance at imaging and may resemble juvenile osteochondritis dissecans (JOCD). Irregular, spiculated, and fragmented ossification has been described and has no pathologic significance. Normal variants

Figure 5. Normal appearance of the distal humeral preossification center in the elbow of a 6-year-old girl. Coronal GRE MR image shows a high-signal-intensity focus in the cartilage of the trochlea that corresponds to the preossification center (arrow).

a. **b.**

Figure 6. Variants of ossification in a 4-year-old boy with knee pain and suspected JOCD. **(a)** Sagittal intermediate-weighted MR image shows fragmentation of the SOC (arrow). This change does not involve the weight-bearing portion, and the adjacent cartilage appears normal. **(b)** Sagittal T2-weighted MR image shows normal bone marrow signal intensity without edema.

of ossification affect the non–weight-bearing portion of the condyles and are not associated with marrow edema (Fig 6) (14).

After the development of the SOC, the medullary cavity contains hematopoietic marrow and demonstrates low signal intensity on T1-weighted images and high signal intensity on water-sensitive images (1). Within 6 months of its development, the marrow in the SOC undergoes fatty transformation and demonstrates high signal intensity on T1-weighted images. This process occurs first in the distal epiphysis and then in the proximal epiphysis (1). In each individual epiphysis, transformation starts in the core of the SOC and progresses toward the periphery, where active endochondral ossification is taking place (Fig 3a) (15). Conversion of marrow follows an analogous pattern in the shaft of the bone, starting at the diaphysis (farthest from the physis) and advancing toward the metaphysis (1). However, this process is more gradual and occurs over several years.

Persistent hematopoietic marrow seen in the epiphysis at MR imaging can be misleading. A hypointense rim seen at the periphery of the SOC on T1-weighted images is normal and results from the centrifugal direction of marrow transformation (15). At times, there are patchy or hemispheric foci of hematopoietic marrow in young children that can persistent even after physeal closure. These foci are especially common in the proximal humerus and femur and are analogous to the flame-shaped areas seen in the metaphysis of young children (1,16). Persistent hematopoietic marrow in the epiphysis has no pathologic significance. Patchy foci of residual hematopoietic marrow

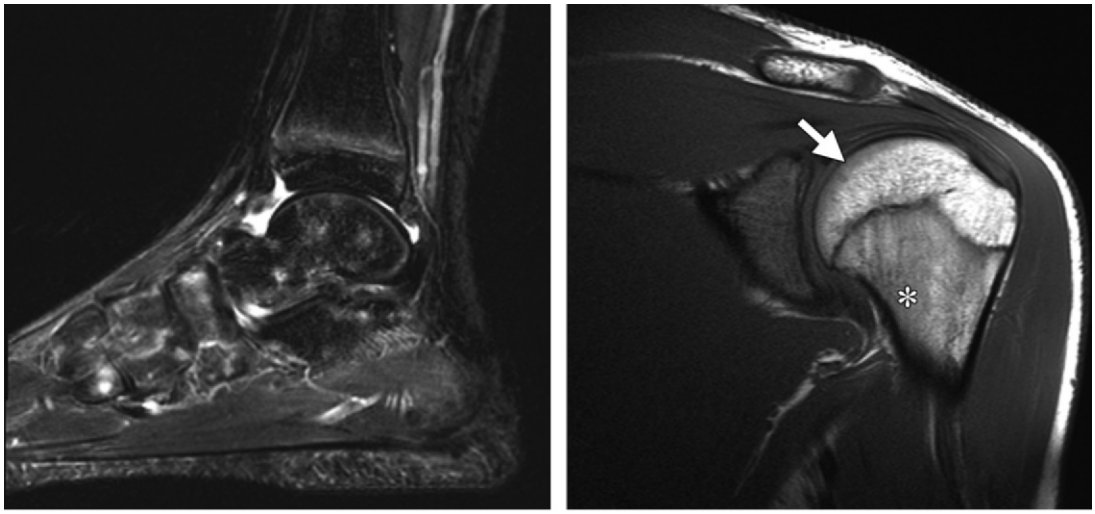

a. b.

Figure 7. Residual hematopoietic marrow. **(a)** Sagittal fat-suppressed T2-weighted MR image of the foot in a 9-year-old girl shows scattered foci of high signal intensity in the tarsal bones. These foci correspond to persistent red marrow and can be seen in healthy children. **(b)** Coronal T1-weighted MR image of the shoulder in a 16-year-old male adolescent shows low signal intensity in the peripheral aspect of the humeral head (arrow). The signal intensity is similar to that of the red marrow in the proximal humeral metaphysis (*).

also can be seen in the tarsal and carpal bones of asymptomatic children and decrease in frequency with age (17). These foci demonstrate high signal intensity on T2-weighted images and are often seen bilaterally, predominantly in endosteal regions. The signal intensity of persistent hematopoietic marrow on T1-weighted images should always be higher than that of muscle because hematopoietic marrow contains approximately 40% fat (Fig 7) (1,12). Marrow that demonstrates signal intensity lower than that of muscle on T1-weighted images is always abnormal.

Contrast-enhanced MR Imaging

At MR imaging, gadolinium-based contrast agents will demonstrate the perfusion of different epiphyseal structures. After intravenous contrast agent administration, a band with early and brisk enhancement in the juxtaphyseal metaphysis likely corresponds to the metaphyseal spongiosa (1). Hematopoietic marrow is more richly vascularized than fatty marrow (15); hence, the metaphysis of young children enhances avidly. The SOC also enhances, although to a lesser extent. The physis shows a subtle enhancement that is more obvious in younger individuals. On postcontrast images, thin linear structures that correspond to the cartilage canals can be appreciated as they course through the low-signal-intensity epiphyseal cartilage (3). The cambial layer of the periosteum is richly vascularized and also has discrete enhancement. Pixel-by-pixel MR subtraction images (contrast-enhanced signal intensity – unenhanced signal intensity) can be obtained. Regions that are intrinsically hyperintense on T1-weighted images will have high signal intensity on pre- and postcontrast-enhanced images but not on subtraction images. Areas of high signal intensity on subtraction images represent enhancement. Subtraction images can better demonstrate subtle changes in enhancement and can make perfusion abnormalities more conspicuous (Fig 8). In summary, contrast-enhanced MR imaging allows evaluation of the microvascular physiology of tissues because enhancement seen on early phase contrast-enhanced images reflects perfusion and vascularity.

A technique called delayed gadolinium-enhanced MR imaging of cartilage (dGEMRIC) can be used to evaluate the molecular composition of the articular cartilage matrix (18). The use of this technique has only been validated in articular cartilage; in the cartilage of the epiphysis and physis, vascular and cellular components interfere with GAG evaluation. GAGs and gadopentetate dimeglumine ($Gd\text{-}DTPA^{2-}$) are negatively charged at physiologic pH. Consequently, the distribution of $Gd\text{-}DTPA^{2-}$ will be inverse to that of GAGs. A T1 map obtained 1 hour after contrast agent administration will demonstrate T1 shortening in GAG-depleted regions, a finding that represents early degenerative changes (18). In cases of developmental dysplasia of the hip and other childhood conditions, dGEMRIC has been used to evaluate cartilage degeneration.

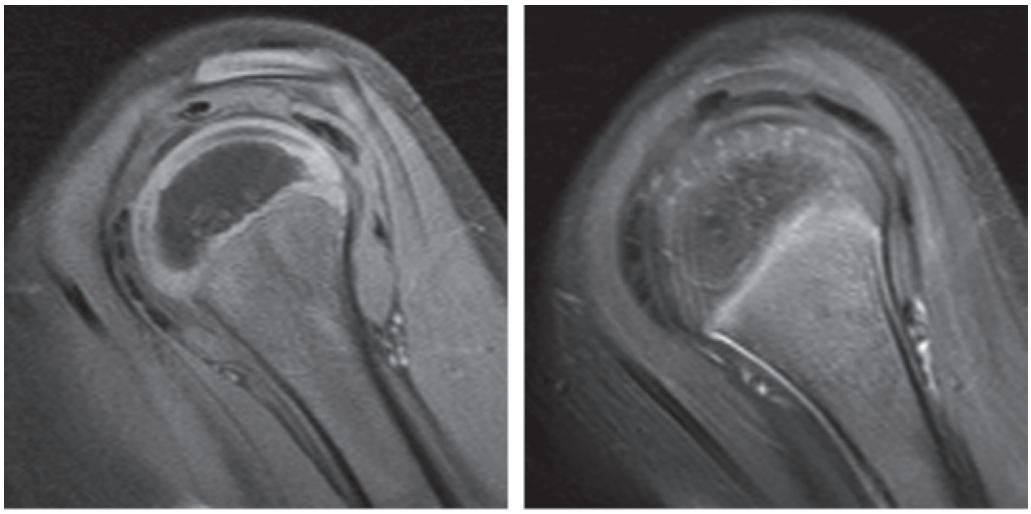

a. b.

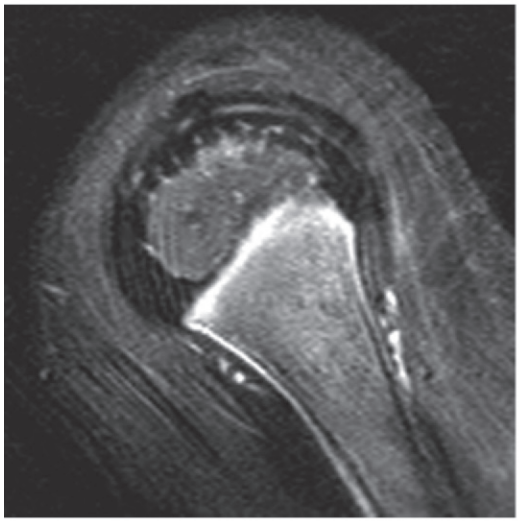

c.

Figure 8. Normal findings on MR images of the shoulder in a 5-year-old boy with shoulder pain. **(a)** Sagittal fat-saturated T1-weighted MR image demonstrates low signal intensity in the epiphysis, a finding compatible with normal fat saturation. **(b)** Sagittal postcontrast T1-weighted MR image shows normal enhancement of the ossified epiphysis, with depiction of the epiphyseal vessels in the epiphyseal cartilage, physis, and vascular periosteum. **(c)** Sagittal MR subtraction image confirms enhancement in the osseous epiphysis and clearly depicts the normal epiphyseal vessels in the epiphyseal cartilage. Marrow enhancement is also seen.

Metaphyseal-like Physiology

Teaching Point

The outermost region of the SOC is richly vascularized, contains hematopoietic marrow, and is a site of endochondral ossification. Physiologically, this region is equivalent to a metaphysis and responds similarly to insults. For example, the hypervascular area at the periphery of the SOC is vulnerable to blood-borne diseases and can be affected by infection. Reconversion from fatty to hematopoietic marrow, such as that observed with colony-stimulating factors and anemias, usually follows the reverse order of normal transformation. Hence, reconversion in the epiphysis starts in the periphery and advances toward the center. At imaging, Harris-Park growth recovery lines can be observed in the epiphysis after a systemic insult has affected the rate of growth. In the SOC, the Harris-Park lines are circular instead of longitudinal because of the spherical shape of the secondary physis (Fig 9).

Pathologic Conditions

Developmental

Developmental Dysplasia of the Hip.—Developmental dysplasia of the hip (DDH) describes a condition in which the femoral epiphysis has an abnormal relationship to the acetabulum. The development of the femoral head and acetabulum are intimately related, and appropriate maturation of the hip depends on a stable, well-located femoral epiphysis (19). The incidence of DDH has been reported as 1.5–20 per 1000 births (20). The cause is uncertain but is considered multifactorial because a combination of anatomic and hormonal influences can alter normal hip development. Mechanical conditions such as oligohydramnios, breech positioning, neuromuscular disorders, and postnatal swaddling in adduction with the hips extended contribute to DDH. A family history of a parent or sibling with DDH is another risk factor that warrants screening ultrasonography (US) (19). The prevalence of DDH is nine times higher in girls because they are more susceptible to the maternal hormones

Figure 9. Metaphyseal-like phenomena in the periphery of the SOC. **(a)** Sagittal T1-weighted MR image of the knee in a 13-year-old male adolescent with sickle cell disease shows reconversion of the red marrow (arrow) in the periphery of the SOC. Reconversion occurs in the reverse order of normal marrow transformation. The metaphyses of the tibia and femur also contain hematopoietic marrow. **(b)** Sagittal T1-weighted MR image demonstrates Harris-Park growth recovery lines in the epiphysis (arrow) and metaphysis (arrowheads) in an 11-year-old girl after fracture of the fibula (not shown). **(c)** Sagittal T2-weighted MR image of the knee in a 9-year-old boy shows an abscess (primary epiphyseal osteomyelitis) that originates in the periphery of the SOC and extends into the cartilage (arrow). The periphery of the SOC has metaphyseal-like vascularity and is prone to blood-borne disease.

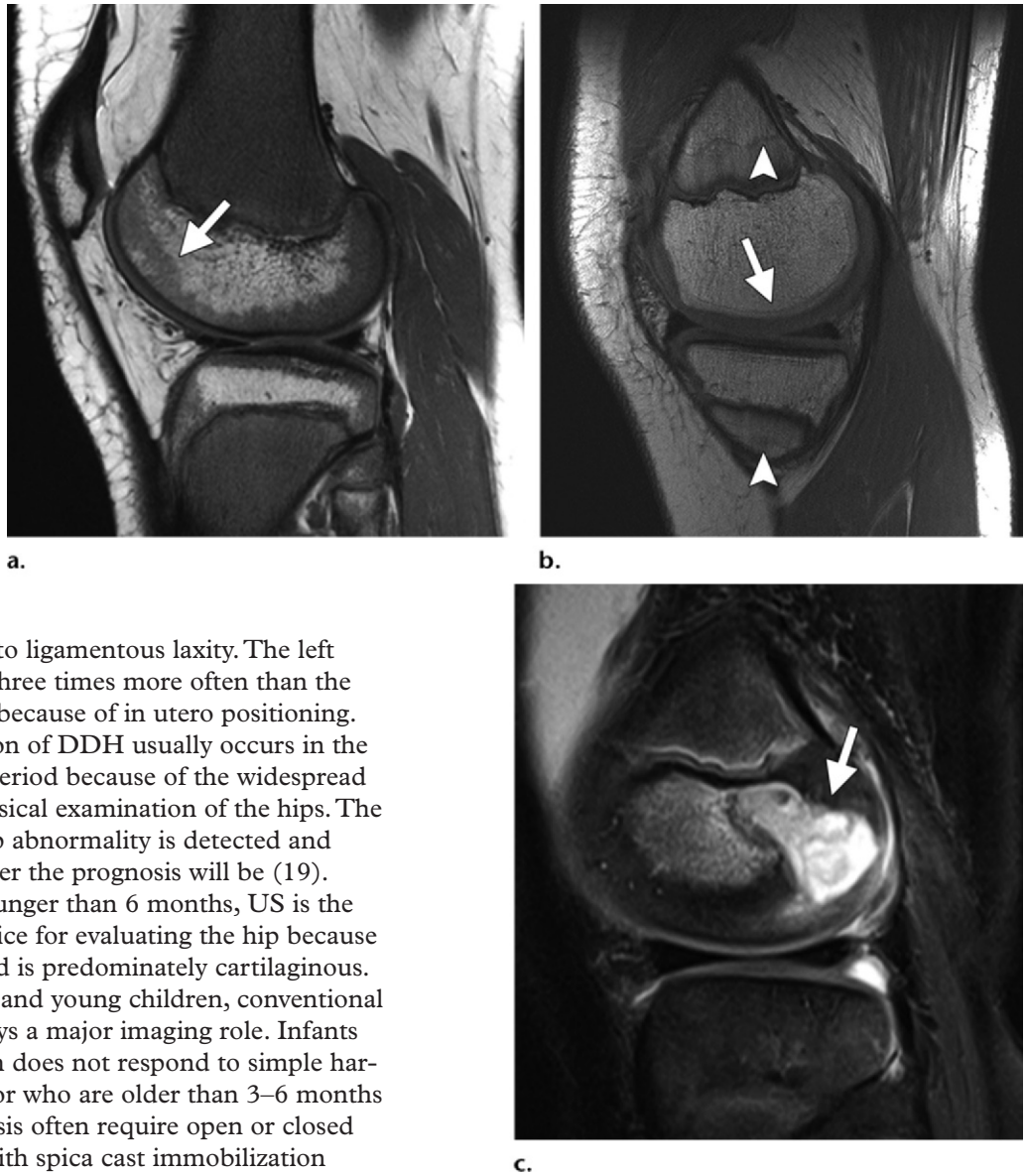

that contribute to ligamentous laxity. The left hip is involved three times more often than the right hip, likely because of in utero positioning. Clinical detection of DDH usually occurs in the early neonatal period because of the widespread adoption of physical examination of the hips. The earlier that a hip abnormality is detected and treated, the better the prognosis will be (19).

In infants younger than 6 months, US is the modality of choice for evaluating the hip because the femoral head is predominately cartilaginous. In older infants and young children, conventional radiography plays a major imaging role. Infants whose condition does not respond to simple harness treatment or who are older than 3–6 months at initial diagnosis often require open or closed hip reduction with spica cast immobilization (21). In these cases, MR imaging is an invaluable method for evaluating whether the hip remains reduced after placement of the spica cast. MR imaging also depicts obstacles to reduction, including femoral head and acetabular incongruency, labral interposition, capsular invagination by the iliopsoas tendon, fibrofatty pulvinar, and hypertrophy of the ligamentum teres of the transverse acetabular ligament.

Treatment of severe DDH involves immobilization of the hip in abduction to allow the reduced stable femoral head to continue remodeling the acetabulum. Unfortunately, maintaining the femoral head in significant permanent abduction with a spica cast leads to avascular necrosis in more than 20% of cases, and this complication is usually detected after it results in osseous deformity. Because treatment is often performed before the appearance of the proximal femoral ossification center, gadolinium-enhanced MR imaging can be used to detect abnormal blood flow to the cartilaginous

Figure 10. Developmental dysplasia of the left hip in a 1-year-old girl. Images were obtained immediately after closed hip reduction with spica cast placement. **(a)** Axial postcontrast fat-saturated T1-weighted MR image shows a small left femoral head with reduced enhancement (arrow) compared to that of the normal contralateral hip. **(b)** Axial MR subtraction image better demonstrates the asymmetry in perfusion, with absent enhancement of the left femoral head (arrow) and normal enhancement of the right femoral head.

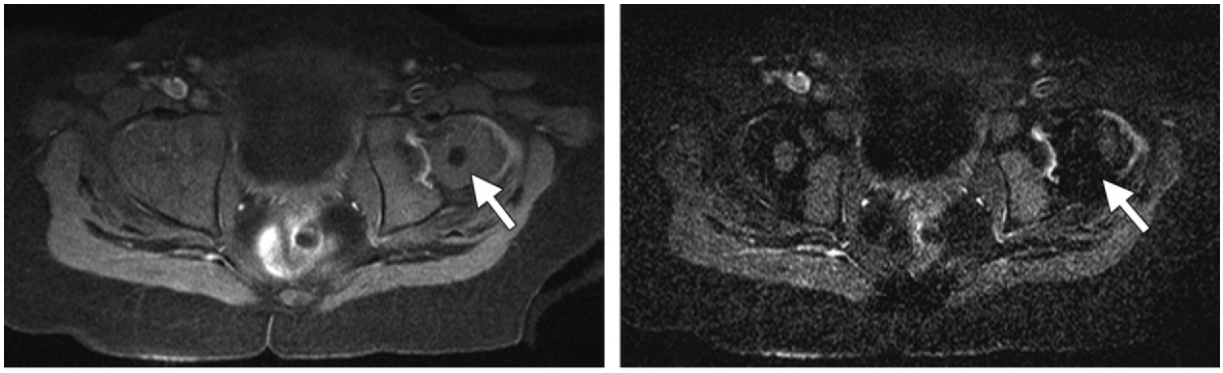

a. b.

proximal femoral epiphysis immediately after a closed reduction. When DDH is unilateral, the unaffected hip can serve as a control for normal perfusion at imaging evaluation. A normal pattern of enhancement at imaging demonstrates the vascular canals of the epiphyseal cartilage and primary spongiosa of the metaphysis (3,22). A patchy pattern of enhancement appears not to have a predictive value for subsequent osteonecrosis. However, a global significant decrease in or total absence of enhancement of the femoral epiphysis is associated with a 10-fold increase in the odds of developing avascular necrosis (Fig 10) (23). MR imaging is optimally performed within 6 hours of surgery to allow manipulation of the cast, if necessary.

Shoulder Dysplasia.—Developmental shoulder dysplasia is most commonly caused by brachial plexus palsy due to a traction injury to the nerve roots of the brachial plexus (C5–T1) during delivery. The incidence of this condition has been reported as 1–1.5 per 1000 live births (24). Predisposing factors include shoulder dystocia, breech presentation, instrumental delivery, and fetal macrosomia. The clinical diagnosis is made by observing arm weakness within a brachial plexus distribution at birth (24).

Most infants recover within the first 3 months of life and improve to nearly normal function, but approximately one-third of patients are left with residual dysfunction. The most common deficit involves weakness of the external rotators of the shoulder (the infraspinatus and teres minor muscles), which are innervated by the supraspinatus and axillary nerves (C5-C6 nerve roots). Prolonged weakness of the external rotator muscles leads to an internal rotation shoulder contracture; periarticular capsuloligamentous tightness; and, over time, a hypoplastic, posteriorly displaced humeral head (25). If it is untreated, brachial plexus palsy may result in shoulder dislocation and a fixed articular deformity of both the glenoid and humeral heads, with subsequent overgrowth of the coracoid (26).

The glenohumeral joint does not completely ossify until puberty. Thus, MR imaging is the preferred method to evaluate the largely cartilaginous humeral head and glenoid in children younger than 5 years. Evaluation with computed tomography may be useful in older children (27). Imaging should include both shoulders to allow comparison with the normal shoulder. High-resolution GRE MR imaging sequences best demonstrate the high-signal-intensity hyaline cartilage of the humeral epiphyses and glenoid fossae as well as the low-signal-intensity labrum in young infants (25,27). Axial and oblique coronal MR images of the shoulder depict the degree of incongruity of the glenohumeral joint, shape of the humeral head, and extent of glenoid hypoplasia. In addition, glenoid version can be readily measured at MR imaging (27). Advanced shoulder dysplasia manifests as a poorly developed posterior glenoid cavity and labrum, with posterior displacement of the humeral head (Fig 11). Severely affected children will also demonstrate thinning of the superior aspect of the glenoid cartilage and atrophy of the shoulder girdle muscles (27).

Treatment options depend on the patient's age at diagnosis, the extent of glenohumeral dysplasia, and the reducibility of the subluxation or dislocation (if present). Appropriate intervention is aimed at achieving full passive range of motion, maintaining a stable glenohumeral articulation, and facilitating muscle rebalancing to enhance glenoid remodeling (26).

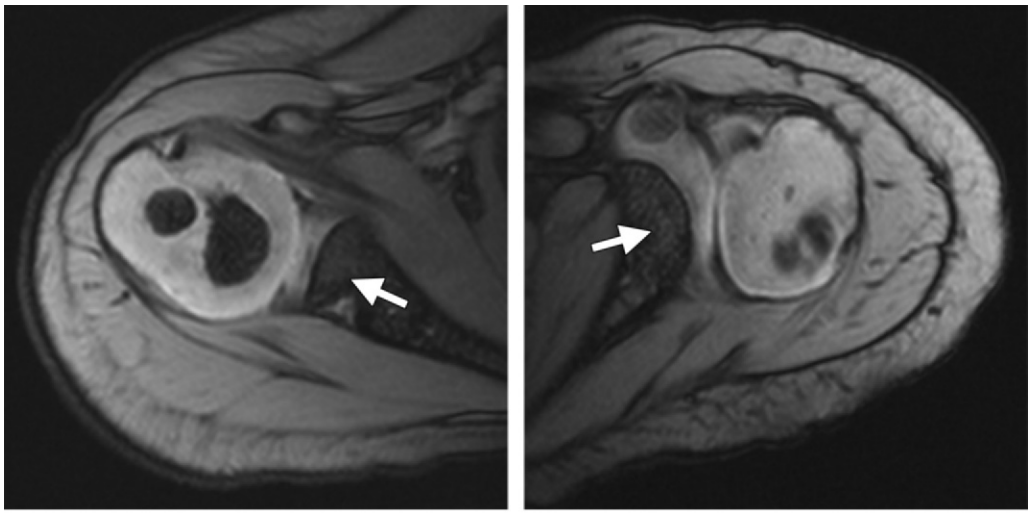

a. b.

Figure 11. Shoulder dysplasia in a 19-month-old boy with left brachial plexus palsy. **(a)** Axial GRE MR image of the normal right shoulder shows a well-formed proximal humeral epiphysis with two partially ossified SOCs. There is a normal glenohumeral relationship with a well-formed glenoid (arrow). **(b)** Axial GRE MR image of the left shoulder demonstrates posterior-inferior subluxation of the humeral head, with glenoid hypoplasia (arrow) and a deficient labrum seen posteriorly. The humeral head is small, with delayed maturation of the SOCs.

Blount Disease.—Blount disease, a developmental abnormality of endochondral ossification in the medial proximal tibial physis, causes maldevelopment of the proximal tibial epiphysis and varus and procurvatum deformity of the tibia. Blount disease can ultimately lead to gait deviations, limb-length discrepancy, and premature arthritis (28). Early-onset, or infantile, Blount disease develops before the age of 4 years, whereas late-onset disease is characterized as juvenile (4–10 years of age) or adolescent (after 10 years of age). Bilateral involvement is common and more typically affects obese children of African American or Scandinavian descent. Because of the significant association of elevated body-mass index with the need for surgical intervention, biomechanics is thought to play a role in morbidity (29).

Anteroposterior radiographs of the knees obtained with the patient in a standing weight-bearing position are used for initial evaluation for Blount disease, and MR imaging is reserved for advanced cases or patients for whom surgery is planned. Early in the disease process, the medial proximal tibial physis becomes widened because of disruption to endochondral ossification. This is followed by delayed ossification of the medial tibial epiphysis and secondary sloping of the medial physis. The medial meniscus often becomes enlarged and demonstrates increased signal intensity on MR images (Fig 12) (30). In patients with significant physeal injury, a bony bridge may form.

Dysplasia Epiphysealis Hemimelica.—Dysplasia epiphysealis hemimelica (DEH), also known as Trevor disease, is a rare developmental disorder characterized by a lobulated osteochondral overgrowth in the developing epiphysis (31). The asymmetric growth usually is confined to either the medial or lateral aspect of the affected epiphysis. Histologic examination demonstrates a mass protruding from the epiphysis, with a cartilaginous cap reminiscent of that seen in osteochondromas. The bone and cartilage in the lobulation are disorganized and contain multiple areas of endochondral ossification (31). The prevalence of DEH is three times higher in boys than in girls, and DEH most often affects the lower extremities and the medial aspect of the joints (32).

DEH can manifest in three clinical forms: localized DEH, which affects only one epiphysis; classic DEH, which affects more than one epiphysis in a limb; and generalized or severe DEH, which affects all epiphyses in a limb (33). DEH usually manifests during childhood as pain in the affected joints or a palpable mass. With disease progression, growth arrest due to physeal involvement and angular deformity caused by overgrowth can develop (31). Because DEH has no malignant potential, treatment is aimed at reducing pain and addressing deformities that affect mechanical function. Simple surgical excision yields positive results and can help prevent joint degeneration.

MR imaging is used to diagnose DEH, show the extent of epiphyseal involvement, and evaluate the articular cartilage. Abnormal cartilage

a. b.

Figure 12. Blount disease in a 4-year-old girl. Coronal GRE **(a)** and coronal T1-weighted **(b)** MR images show down-sloping of the medial aspect of the tibial physis (arrow) and abnormal high signal intensity in the epiphyseal cartilage (arrowhead in **a**). The medial meniscus is enlarged, and the physis is interrupted medially. Varus angulation of the tibia is also seen.

Figure 13. Trevor disease in an 8-year-old boy with knee pain. Coronal T1-weighted MR image of the left knee shows a normal lateral condyle (arrowhead). The medial condyle shows abnormal overgrowth of the SOC (white arrow). Fragmentation of the tibial SOC is also seen (black arrow).

has intermediate signal intensity on T1-weighted images and high signal intensity on T2-weighted images. As the lesion matures and calcifies, low-signal-intensity foci are seen on images obtained at all pulse sequences, and a cartilaginous cap with high signal intensity on T2-weighted images becomes more conspicuous. Eventually the mass ossifies and fuses with the SOC. The signal intensity of mature lesions usually resembles that of normal marrow (Fig 13). High signal intensity secondary to mechanical stress can be appreciated in the affected epiphysis, articulating bones, and surrounding soft tissues (32).

Köhler Disease.—Köhler disease is a rare osteochondrosis or apophysitis of the tarsal navicular bone with a poorly understood etiology (34). It occurs in children aged 3–10 years and is three times more common in boys. Köhler disease is usually unilateral and resolves spontaneously. Diagnosis at radiography is challenging because both the normal navicular and the navicular in Köhler disease can appear fragmented, irregular, and sclerotic (35). MR imaging can help distinguish Köhler disease from normal variations of the navicular by demonstrating inflammation. The navicular will demonstrate low signal intensity on T1-weighted images, high signal intensity on water-sensitive images (36), and a lack of gadolinium contrast enhancement (Fig 14). In symptomatic children, treatment with rest and sometimes a short-leg cast usually leads to resolution without sequelae (34).

Trauma

Acute Trauma to the Physis.—Physeal fractures are an important cause of morbidity before skeletal maturity. In children, 15%–30% of fractures affect the physis, and 15% of these result in growth disturbance (37). Abnormal growth can result from direct damage to the physis or the formation of a physeal bony bridge that tethers growth. Bridges develop because of abnormal

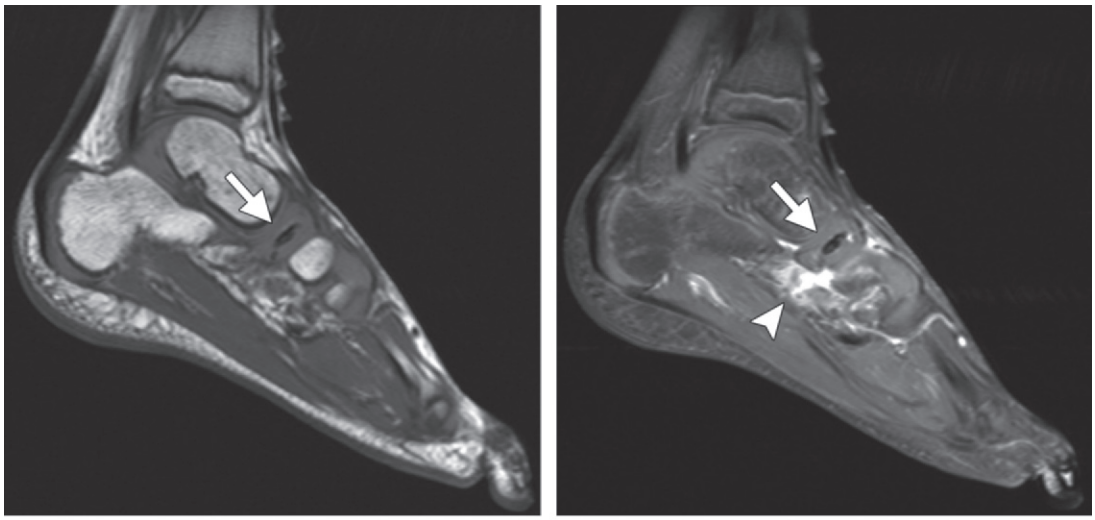

a. b.

Figure 14. Köhler disease in a 7-year-old boy with a limp. **(a)** Sagittal T1-weighted MR image of the foot shows a small low-signal-intensity ossification center in the navicular (arrow) **(b)** Sagittal postcontrast T1-weighted MR image demonstrates absence of enhancement in the navicular (arrow) and edema in the surrounding soft tissues (arrowhead).

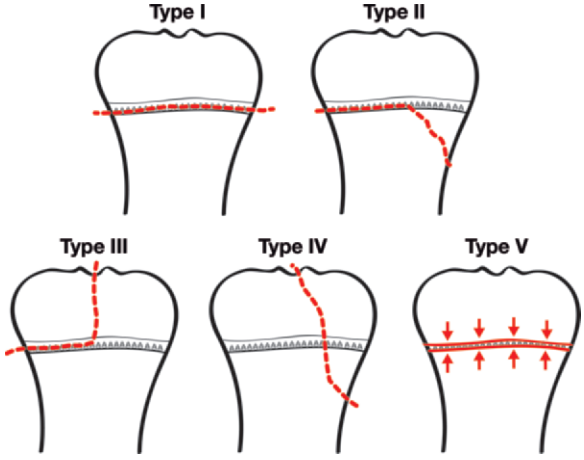

Figure 15. Diagram illustrates the Salter-Harris classification of physeal fractures. Dashed red lines show the pathway of the fracture. In the Salter-Harris type V fracture, arrows represent compressional forces.

communication between the epiphyseal and metaphyseal vessels. Physeal Salter-Harris fractures (Fig 15) are divided into two categories on the basis of the involved physeal regions: *(a)* horizontal fractures without involvement of the germinal or proliferative zone of the physis and *(b)* longitudinal fractures that extend through all zones of the physis into the epiphysis. Horizontal fractures (Salter-Harris types I and II) result in bridge formation in 25% of cases, whereas longitudinal fractures (Salter-Harris types III and IV) result in bridge formation in 75% of cases. The specific physis affected by the fracture, however, is the main determinant of the subsequent risk of growth arrest. For example, fractures of the distal femur and proximal tibia, although uncommon (1.4% and 0.8% of all physeal fractures, respectively), result in 35% and 16% of bony bridge formations, respectively. In contrast, injuries that involve the most common locations of physeal fractures, the phalanges (37.4%) and distal radius (17.9%), seldom result in growth arrest (8,38).

Teaching Point

MR images clearly depict the linear course of a fracture. In the bone, a fracture usually is surrounded by substantial marrow edema, which has high signal intensity on water-sensitive MR images and low signal intensity on T1-weighted images. As the fracture violates the physis, the normal trilaminar appearance on water-sensitive MR images is lost. In the epiphyseal cartilage, the fracture line is best demonstrated on T2-weighted and proton-density–weighted MR images (39) (Fig 16). The use of a gadolinium-based contrast agent is not necessary.

MR imaging also allows early detection of a physeal bridge. Focal loss of the normal signal intensity of the physis is an early indication of a developing bridge (8). This change is particularly conspicuous on high-resolution GRE MR images, which depict the physis with high signal intensity and the developing bony bridge with very low signal intensity (12). Most bridges occur in areas of physeal undulation, such as the center of the distal femoral physis and the medial aspect of the distal tibial physis (the Kump bump) (Fig 17) (8). Areas of normal physeal undulation should not be mistaken for a bridge. Factors associated with a worse prognosis include fracture severity

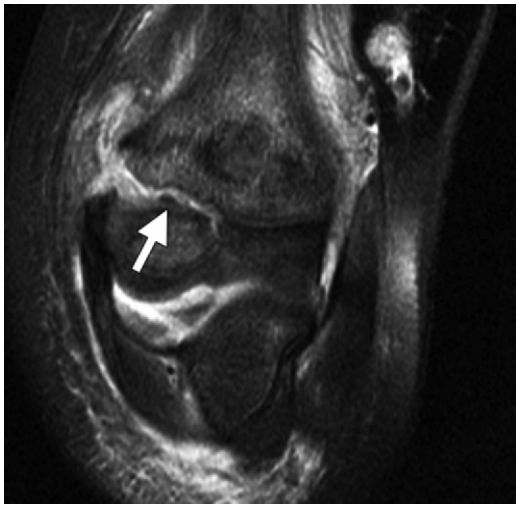

Figure 16. Lateral condylar fracture in the elbow of a 5-year-old boy. Coronal fat-suppressed T2-weighted MR image shows a fracture affecting the distal humeral physis and metaphysis that extends into the cartilaginous epiphysis (Salter-Harris IV) (arrow). A small joint effusion and adjacent soft-tissue edema are also seen.

a. **b.**

Figure 17. Salter-Harris III fracture sequelae in the distal tibia of a 13-year-old male adolescent. Coronal intermediate-weighted **(a)** and sagittal GRE **(b)** MR images of the ankle show loss of continuity of the physis in the anteromedial region of the distal tibia with a bony bridge (arrow in **a** and **b**).

(ie, comminution or displacement), younger age, growth potential of the involved physis, and size of the bony bridge. If a bony bridge develops, three-dimensional reconstructions obtained from isotropic GRE MR imaging sequences can be used to map the bridge, determine the percentage of surface area affected, and guide treatment (8). Small bridges may resolve spontaneously, whereas larger ones may require surgical resection. Although no definitive treatment guidelines exist, children with an established or developing deformity who have 2 years or 2 cm of remaining growth should be considered as candidates for bridge resection (40).

Chronic Physeal Trauma.—Repetitive trauma, such as that sustained by elite adolescent athletes, may result in chronic damage to the physes. Chronic stress to the physis disrupts the metaphyseal vessels, interferes with endochondral ossification, and results in physeal chondrocytes remaining in the metaphysis (41). Sports-related activities can affect certain joints. Physeal knee injuries occur in soccer, tennis, and football players; wrist injuries occur in gymnasts; and injuries to the proximal humeral physes occur in baseball players (42). Patients often present with chronic pain at the site of the specific overuse injury (11,12), and the injury can progress to growth

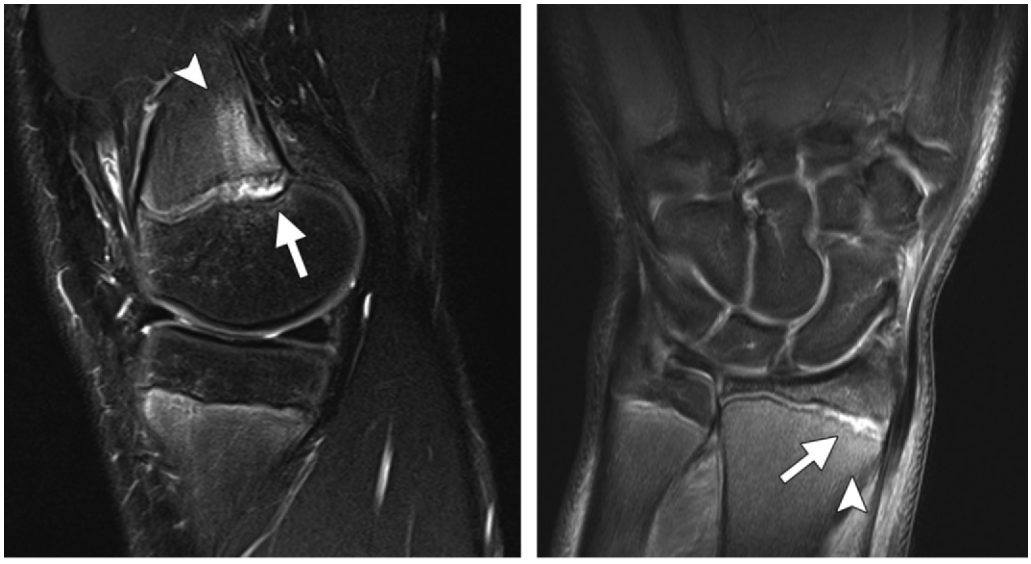

a. b.

Figure 18. Chronic physeal trauma. Sagittal T2-weighted MR image of the knee in a 12-year-old male soccer player **(a)** and sagittal intermediate-weighted MR image of the wrist in a 13-year-old male football player **(b)** show widening and irregularity of the physis (arrow in **a** and **b**), with increased signal intensity in the adjacent metaphysis (arrowhead in **a** and **b**).

abnormalities and consequent deformity if the stressor is not removed (41).

On MR images, the affected physis is widened and irregular and demonstrates increased signal intensity on T2-weighted images. The ZPC often is effaced (Fig 18). In gymnasts with repetitive injury to the distal radius, a decreased rate of distal radial growth can result in positive ulnar variance and associated tears in the triangular fibrocartilage (43). Early identification of these abnormalities allows proper rehabilitation and changes to activity patterns before permanent sequelae ensue (42).

Acute Osteochondral Injuries.—Acute osteochondral injuries are the most common abnormality found in older children and adolescents with suspected internal derangement of the knee (44). Because of increased participation by children and adolescents in high-level sports activities, the prevalence of such injuries is increasing. Patients often present with intermittent joint pain and locking after trauma. Femoral lesions are more common before physeal closure, whereas patellar lesions are more common afterward (44). In the setting of traumatic patellar dislocation, osteochondral injuries in the inferomedial patella and lateral femoral condyle and free osteochondral fragments are seen at imaging in 38%, 38%, and 42% of patients, respectively (45).

The Outerbridge classification can be used to describe and classify acute osteochondral injuries at MR imaging (44,46). A type 1 injury displays thickening of the articular cartilage with abnormal signal intensity; type 2 shows superficial loss of cartilage thickness or fissuring; type 3 shows deep loss of cartilage thickness or fissuring; type 4 is a "full-thickness" injury with abnormal signal intensity of the subchondral bone; and type 5 is associated with a free osteochondral fragment (Fig 19). Type 1 and type 2 injuries are especially difficult to diagnose because there are no abnormalities in the signal intensity of the underlying bone (44). It is important to recognize these injuries at imaging because they increase the risk of early joint degeneration. Osteochondral injuries have a better prognosis in children and adolescents because a growing child is able to repair the cartilage damage better than an adult is.

Juvenile Osteochondritis Dissecans.—JOCD is a disease that manifests before physeal closure and results in destruction of the subchondral bone and articular surface (47). Given its distinct clinical course, JOCD is considered to be different from adult osteochondritis dissecans. Repetitive trauma has been postulated as the most likely cause of JOCD. Recent studies suggest that chronic epiphyseal trauma disrupts endochondral ossification at the secondary physis (47) through a mechanism similar to that of stress injuries to the primary physis (41). Genetic factors, ischemia, and ossification abnormalities also play a role (48).

JOCD usually presents between the ages of 10–15 years, when children tend to be more active. Males are affected (60%–80%) more often than females (49). Symptoms include pain, clicking or catching of the joint, and loss of function due to intra-articular loose bodies. The most commonly

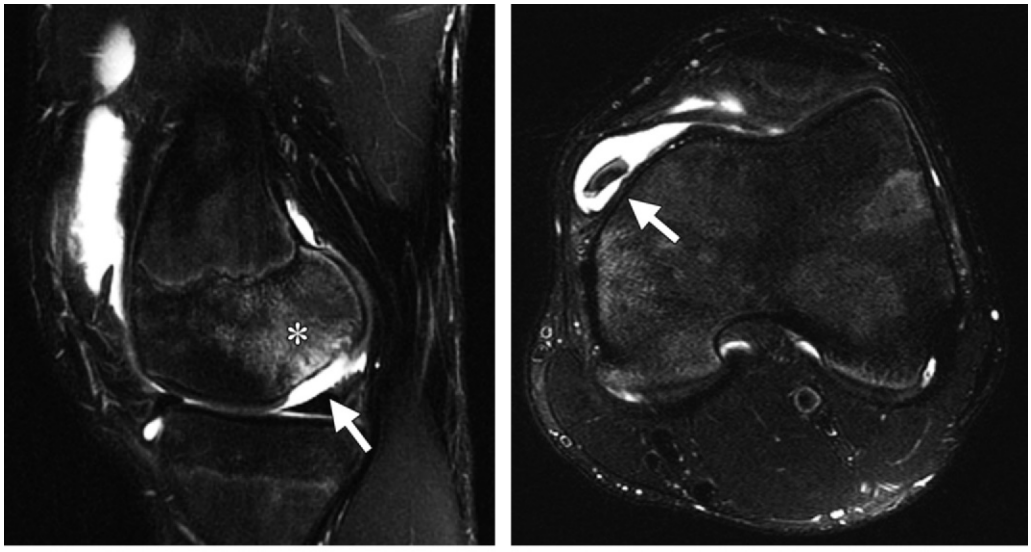

a. b.

Figure 19. Acute osteochondral injury in a 16-year-old male adolescent that was sustained while playing basketball. **(a)** Sagittal fat-suppressed T2-weighted MR image of the knee shows an osteochondral defect in the posterior third of the femoral epiphyseal cartilage (arrow) with associated bone edema (*). **(b)** Axial fat-suppressed T2-weighted MR image at the level of the distal femur shows a loose osteochondral body (arrow) and joint fluid.

affected joint is the knee, followed by the ankle, elbow, shoulder, and hip (49). In the knee, the most common location is the posterolateral aspect of the medial femoral condyle (51%). The weight-bearing portion of the medial femoral condyle and the medial aspect of the lateral femoral condyle are affected in 19% and 7% of cases, respectively. The patella infrequently is affected (48). If JOCD is untreated, an osteochondral fragment can detach from the osseous bed and result in loss of articular surface congruence, loose bodies, and early joint degeneration.

MR imaging is used to help establish diagnosis, determine lesion stability, and assess the need for treatment. MR imaging criteria for lesion instability include a line of high signal intensity on T2-weighted images between the fragment and the parent bone, cysts near the lesion, a fracture in the articular cartilage, and a fluid-filled osteochondritis dissecans lesion (50). Recent work suggests that a rim of high T2 signal intensity predicts instability only when it has fluid signal intensity and is surrounded by a low-signal-intensity rim. In addition, cysts predict instability only when they are multiple or very large (>5 mm) (Fig 20) (51). Recent evidence suggests that some of the rounded regions of high signal intensity seen on MR images could correspond to cartilage rather than to cysts. Small lesions that are deemed stable at MR imaging (low-grade lesions) can be managed conservatively with rest and restricted weight bearing. Large lesions or those with features that suggest instability (high-grade lesions) usually require intervention, which can include drilling to stimulate healing, in-situ fixation, and autologous transplantation in severe cases (49).

Infection

Acute Osteomyelitis.—In children, acute osteomyelitis is most commonly acquired hematogenously in the setting of bacteremia. The most commonly isolated organisms are *Staphylococcus aureus*, β-hemolytic *Streptococcus*, *Streptococcus pneumoniae*, *Escherichia coli*, and *Pseudomonas aeruginosa* (10). There has been an increasing incidence of methicillin-resistant *S aureus* (MRSA) and *Kingella kingae* infections in children younger than 4 years (10).

In acute hematogenous osteomyelitis, the pathogen reaches the metaphysis via the nutrient artery. In infants, there is an increased frequency of epiphyseal and joint infections as a result of transphyseal blood flow (10). In children and adolescents aged 2–16 years, very few blood vessels cross from the metaphysis into the epiphysis; therefore, the metaphyses and metaphyseal equivalents are the most common locations for acute hematogenous osteomyelitis (52,53). Less frequently, osteomyelitis can develop primarily in the epiphysis. Primary epiphyseal infection typically arises in the periphery of the SOC at the richly vascularized junction between bone and cartilage (Fig 9c). Epiphyseal osteomyelitis tends to be more chronic and destroys the physis less often than does metaphyseal infection.

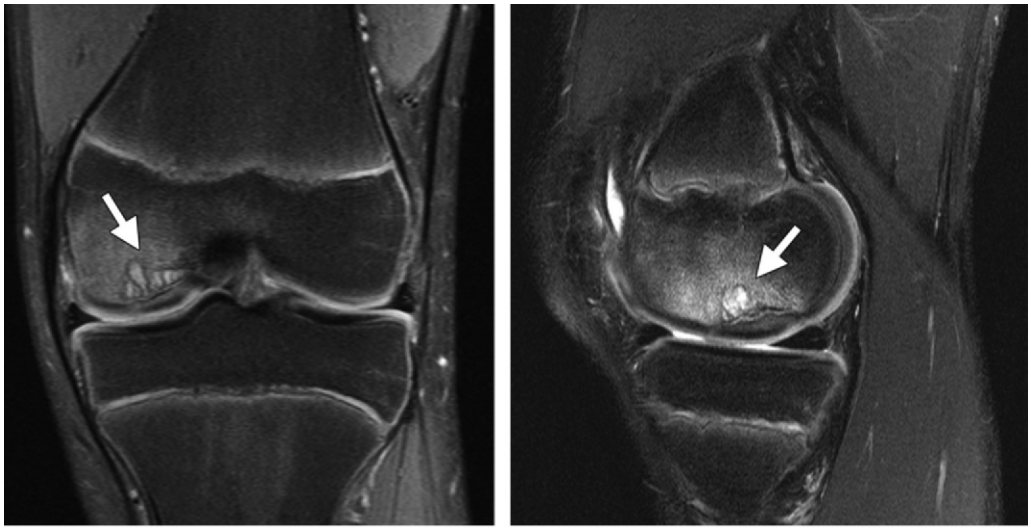

a. b.

Figure 20. JOCD of the medial femoral condyle in a 15-year-old male adolescent with knee pain. **(a)** Coronal fat-saturated intermediate-weighted MR image shows multiple cysts (arrow) in the medial femoral condyle, with adjacent marrow edema. **(b)** Sagittal fat-saturated T2-weighted MR image shows a dominant large cyst (arrow) and rim of high signal intensity beneath the subchondral bone.

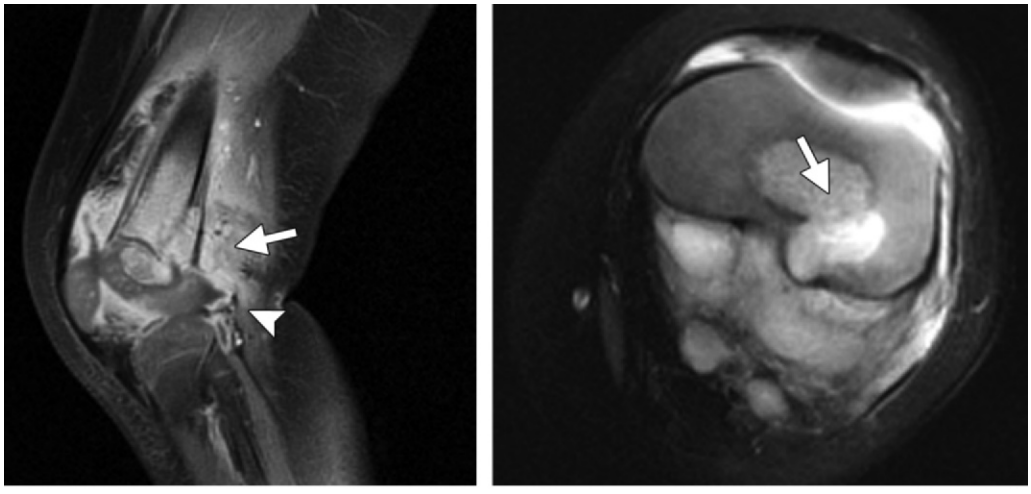

a. b.

Figure 21. Osteomyelitis in a 15-month-old boy. **(a)** Sagittal postcontrast fat-saturated T1-weighted MR image of the knee shows osteomyelitis in the distal femoral metaphysis, with a subperiosteal collection (arrow) that extends to the physis. The epiphyseal cartilage in the posterior aspect of the femoral condyle shows a subtle enhancement defect (arrowhead). **(b)** Axial fat-saturated T2-weighted MR image shows extension of the infection into the epiphyseal cartilage and SOC, with an abscess in the location of the enhancement defect (arrow).

However, the infection can extend into the epiphyseal and physeal cartilage and lead to chronic deformity and growth arrest (52,53).

The clinical manifestation of osteomyelitis in the infant and young child can be diagnostically challenging. Imaging plays a crucial diagnostic role and can aid in management. Plain radiographs primarily serve to exclude other pathologies. Conventional radiographs can demonstrate an obliteration of the fat planes that indicates deep soft-tissue swelling. In cases of primary epiphyseal osteomyelitis, radiographs can demonstrate radiolucency in the affected portion of the SOC. MR imaging can delineate the full extent of disease by characterizing the marrow, cartilage, muscle, and subcutaneous tissues (10).

Evaluation for osteomyelitis includes a combination of T1-weighted and water-sensitive MR imaging sequences. In osteomyelitis, normal bone marrow becomes infiltrated with inflammatory cells

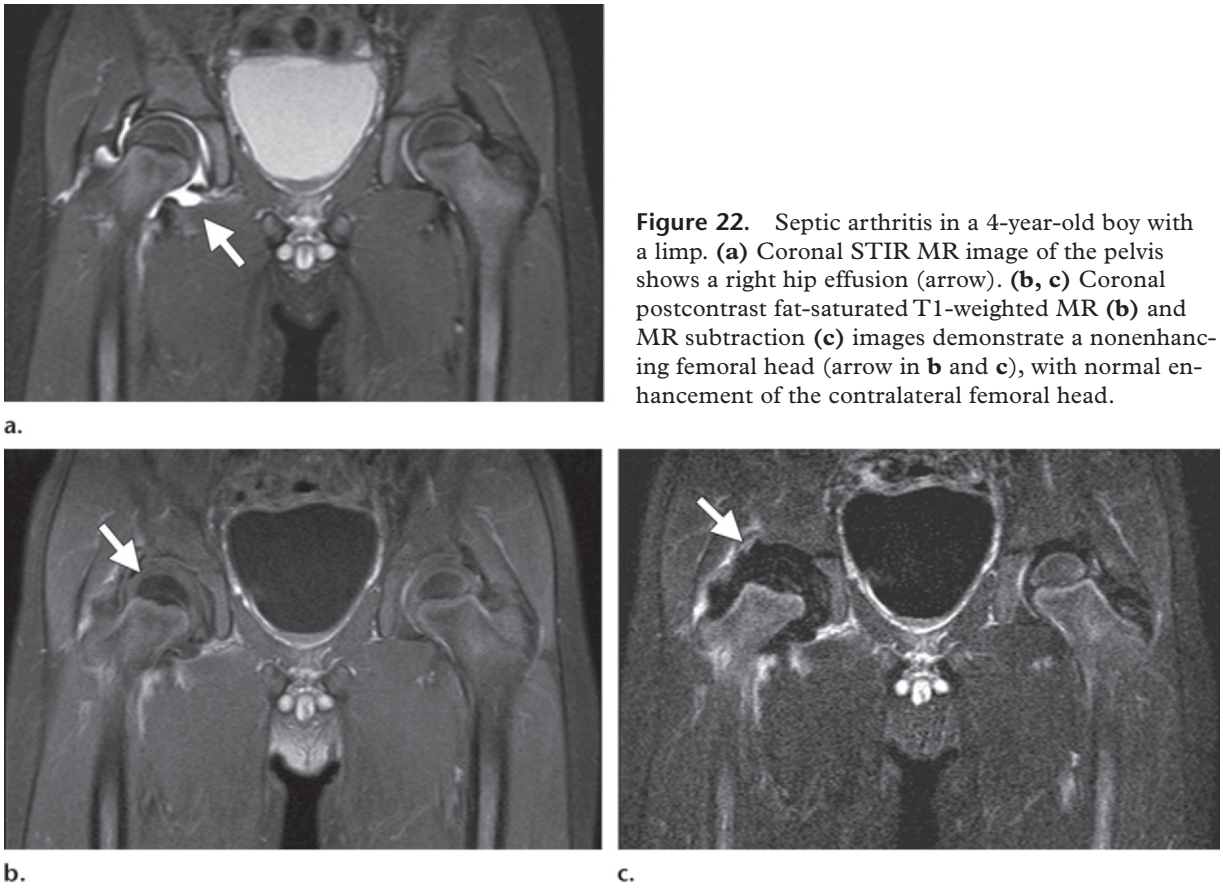

Figure 22. Septic arthritis in a 4-year-old boy with a limp. **(a)** Coronal STIR MR image of the pelvis shows a right hip effusion (arrow). **(b, c)** Coronal postcontrast fat-saturated T1-weighted MR **(b)** and MR subtraction **(c)** images demonstrate a nonenhancing femoral head (arrow in **b** and **c**), with normal enhancement of the contralateral femoral head.

and purulent material that demonstrates low signal intensity on T1-weighted images and high signal intensity on water-sensitive images. Differentiating these changes from normal hematopoietic marrow in children can be challenging. In general, the T2-weighted and STIR MR signal intensity of bone marrow affected by osteomyelitis is higher than that of normal hematopoietic marrow. Gadolinium-enhanced fat-suppressed T1-weighted images aid in detecting intramedullary collections, subperiosteal collections, and soft-tissue abscesses by demonstrating peripheral enhancement of foci with low T1 signal intensity (10). In young children with abundant epiphyseal cartilage, the use of intravenous gadolinium contrast material is crucial. Involvement of the epiphyseal cartilage with abscess formation and destruction of the physis manifests as enhancement defects on postcontrast images (Fig 21). These findings carry a poor prognosis with increased risk of growth arrest. Furthermore, findings at unenhanced T1-weighted or fluid-sensitive MR imaging can appear normal (53).

Teaching Point

Septic Arthritis and the Epiphysis.—Septic arthritis is caused by either hematogenous seeding or direct extension into the joint space in children with osteomyelitis or an adjacent soft-tissue infection. Septic joints are most commonly encountered in neonates and are most often seen in the shoulder or hips, followed by the knee, elbow, and ankle (10). The immature hip is particularly prone to development of septic arthritis because the metaphysis is intracapsular and allows easy spread of infection. Multifocal joint involvement is common in very young patients (54). Common pathogens include *S aureus*, *Streptococcus pyogenes*, *S pneumoniae*, and *Neisseria gonorrhoeae* (10). In young patients, diagnosis is often delayed because of challenges with clinical examination and a lack of localizing symptoms.

MR imaging findings of a septic joint include an effusion, enhancement of thickened synovium, and reactive edema within the adjacent bone. Joint infections may result in subluxation and avascular necrosis of the epiphysis. MR imaging is helpful in detection of an unsuspected epiphyseal infection. The rapid rise in intracapsular pressure that occurs with septic arthritis can interfere with epiphyseal perfusion, particularly in the hip (55). Gadolinium-enhanced T1-weighted MR subtraction images can depict subtle changes in perfusion in the adjacent epiphysis that may indicate a joint at risk for development of avascular necrosis (Fig 22). Appropriate intervention, including open debridement, should be initiated as soon as possible to limit long-term complications.

The sequelae of septic arthritis are variable and depend on the joint affected, patient age at diagnosis, virulence of the organism, and time from symptom onset to treatment (56). Suppurative arthritis that occurs before the appearance of the epiphyseal SOCs generally delays their appearance by months. This process often results in irregular and small ossific nuclei and ultimately a deformed joint. If joint infection occurs after the ossific nuclei are present, the ossific nuclei may undergo osteolysis and gradually redevelop as small irregular nuclei with consequent epiphyseal deformity (57). Flexion contracture and leg-length discrepancy are common sequelae (57).

Vascular

Osteonecrosis.—Osteonecrosis is a condition in which traumatic and nontraumatic insults cause decreased perfusion to the epiphysis and result in cellular death. More than 20,000 new patients are affected each year in the United States (58). The most common site is the hip; other common sites are the knees, shoulders, and ankles. Ischemia of the femoral head accounts for nearly 10% of the 500,000 total hip replacements performed in the United States annually (59). Approximately 10%–20% of cases have no clear identifiable risk factor and are classified as idiopathic osteonecrosis (60). The goal of imaging is to diagnose the disease at its earliest stages so that optimal treatment can be instituted.

In children, osteonecrosis can have many causes. Trauma can disrupt the arterial supply to the epiphysis, as seen with femoral neck fractures. Epiphyseal arterial microvascularity also can be affected by vasculitides such as systemic lupus erythematous or by radiation therapy (61). Elevated pressure within the epiphysis related to venous hypertension contributes to decreased epiphyseal perfusion and osteonecrosis, as seen with abduction immobilization for hip dysplasia (62), Legg-Calvé-Perthes (LCP) disease (63), sickle cell anemia, synovitis, steroid therapy, and marrow storage diseases (eg, Gaucher disease). Intravascular thrombosis, a condition seen with sickle cell disease, can also lead to altered epiphyseal perfusion with subsequent development of osteonecrosis. With ischemia, the marrow cells become edematous and eventually die (11). Removal of the devitalized bone and weakening of the existing bone leads to collapse of the epiphyseal subchondral bone. Eventually a reparative process ensues and leads to reperfusion, with a front of repair surrounding the ischemic region (11). In the growing epiphysis, repair is usually through the established peri-epiphyseal vessels. In some cases, there is reperfusion through neovasculature that develops across the physis and causes growth disturbance.

In the very early phase of osteonecrosis, the marrow fat demonstrates high signal intensity on T1-weighted images, a finding thought to represent stagnant blood (64) that is best shown on fat-suppressed T1-weighted images (65). In the weeks that follow, epiphyseal ischemia leads to bone marrow edema, and epiphyseal signal intensity will decrease on T1-weighted images and increase on water-sensitive MR images. Weakening of the bony epiphysis leads to decreased height of the epiphyseal subchondral bone, which gives rise to a rim of high signal intensity on water-sensitive MR images. Ultimately, further collapse and fibrosis follow and manifest as decreased marrow signal intensity and a fragmented ossified epiphysis that can be of very low signal intensity on both T1-weighted and water-sensitive MR images. A region of infarct is depicted as a serpiginous rim of low signal intensity (Fig 23) or a double line on water-sensitive MR images (63,65).

At several stages of disease, gadolinium-enhanced imaging aids in the evaluation of epiphyseal ischemia. In patients with joint pain, normal radiographic findings, and normal or unclear findings on unenhanced MR images, gadolinium-enhanced imaging can add insight if a lack of epiphyseal enhancement is demonstrated. In children with established osteonecrosis, the pattern of epiphyseal reperfusion can be demonstrated with gadolinium-enhanced imaging (66). As previously described, when the femoral head is reperfused through the physis, transphyseal neovascularity induces ossification and promotes physeal bony bridging, which is related to a poor outcome (66).

Very early epiphyseal ischemia briefly restricts diffusion, but virtually all children with osteonecrosis present with a later stage of cellular breakdown and increased diffusion (67). Therefore, findings of epiphyseal osteonecrosis are better appreciated on apparent diffusion coefficient (ADC) maps. An area of infarct will demonstrate low signal intensity on diffusion-weighted MR images and high signal intensity on ADC maps. Perfusion- and diffusion-weighted MR imaging are both useful because they each convey a different degree of information over time. In osteonecrosis, perfusion is initially decreased and is followed by a later stage of abnormal increased blood flow. Diffusion increases rapidly and remains elevated throughout the disease course (67).

LCP Disease.—LCP disease is an idiopathic childhood hip disorder that leads to osteonecrosis of the proximal femoral epiphysis and possible permanent deformity of the femoral head (63). It has a reported incidence of 0.2–29 per 100,000 children and is more common in Caucasian children.

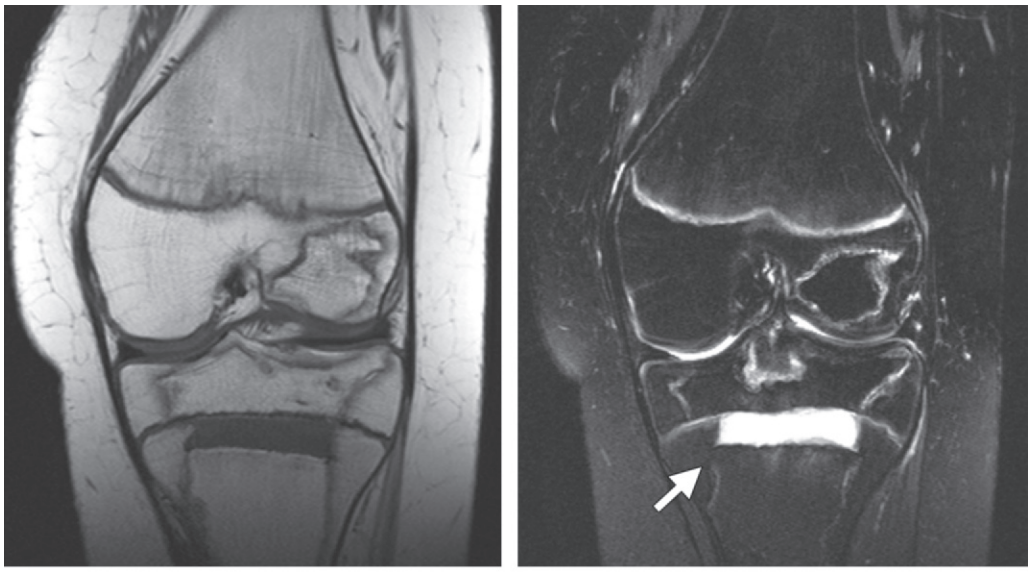

a. b.

Figure 23. Avascular necrosis of the knee in a 13-year-old female adolescent after chemotherapy for acute lymphoblastic leukemia. **(a)** Coronal T1-weighted MR image shows serpiginous areas of low signal intensity in the distal femoral epiphysis, proximal tibial epiphysis, and tibial metaphysis. A low-signal-intensity rim delineates the areas of infarct. The ZPC in the central region of the femoral physis appears effaced and eventually developed a bridge (not shown). **(b)** Coronal T2-weighted MR image shows high-signal-intensity serpiginous rims. A front of unmineralized cartilage that starts in the physis and extends into the tibial metaphysis (arrow) is due to disrupted endochondral ossification.

LCP disease typically affects children aged 5–10 years, with girls being affected slightly earlier. LCP disease is four times more common in boys and is bilateral (typically asynchronous) in 10% of cases. Although the cause is unknown, clinical and experimental evidence suggests that disruption of the blood supply to the growing femoral epiphysis is a key pathogenic event (63). The proposed etiology includes a variety of genetic and environmental factors. Genetic factors such as type II collagen mutation, thrombophilia, and abnormalities in the insulin-like growth-factor pathway predispose children to femoral head ischemia. When susceptible individuals are introduced to environmental conditions such as repeated subclinical trauma or mechanical overloading, LCP disease can be triggered (63).

Teaching Point

Prognostic indicators in LCP disease include age of onset, extent of femoral head deformity and fragmentation, lateral extrusion, physeal involvement, and metaphyseal abnormalities (63,68). Metaphyseal cysts and physeal abnormalities are believed to be predictors of poor outcome. In a study that used multivariate analysis, the probability of subsequent growth arrest was 100% for patients with both epiphyseal and metaphyseal abnormalities, 75% for patients with only physeal interruption, and 50% for patients with only metaphyseal cystic changes (69). In established LCP disease, the reperfusion pattern seen at imaging also has prognostic value. Patients with increased enhancement in the lateral pillar have a good prognosis, whereas transphyseal reperfusion through the remainder of the physis increases the risk of growth arrest (66).

Most children who present with LCP disease have abnormal findings at initial MR imaging, even if the radiographic findings are normal. Because the anterior half of the femoral head is more affected by osteonecrosis, sagittal MR imaging is imperative to evaluate findings that are more prominent anteriorly, such as marrow edema, subchondral fluid, and collapse (70). Abnormalities that are very anterior within the epiphysis or metaphysis are difficult to fully appreciate on coronal images and are best demonstrated on sagittal images. Diffusion-weighted MR imaging may also have an important role in prognosis when there are metaphyseal changes. In LCP disease, increased metaphyseal diffusion is associated with transphyseal reperfusion and an increased risk of growth arrest (Fig 24) (71).

Tumors

Chondroblastoma.—Chondroblastomas are rare, benign, cartilaginous tumors (less than 2% of all bone tumors) that affect the epiphysis of children (72). About 75%–80% of chondroblastomas involve the long bones, and the most common

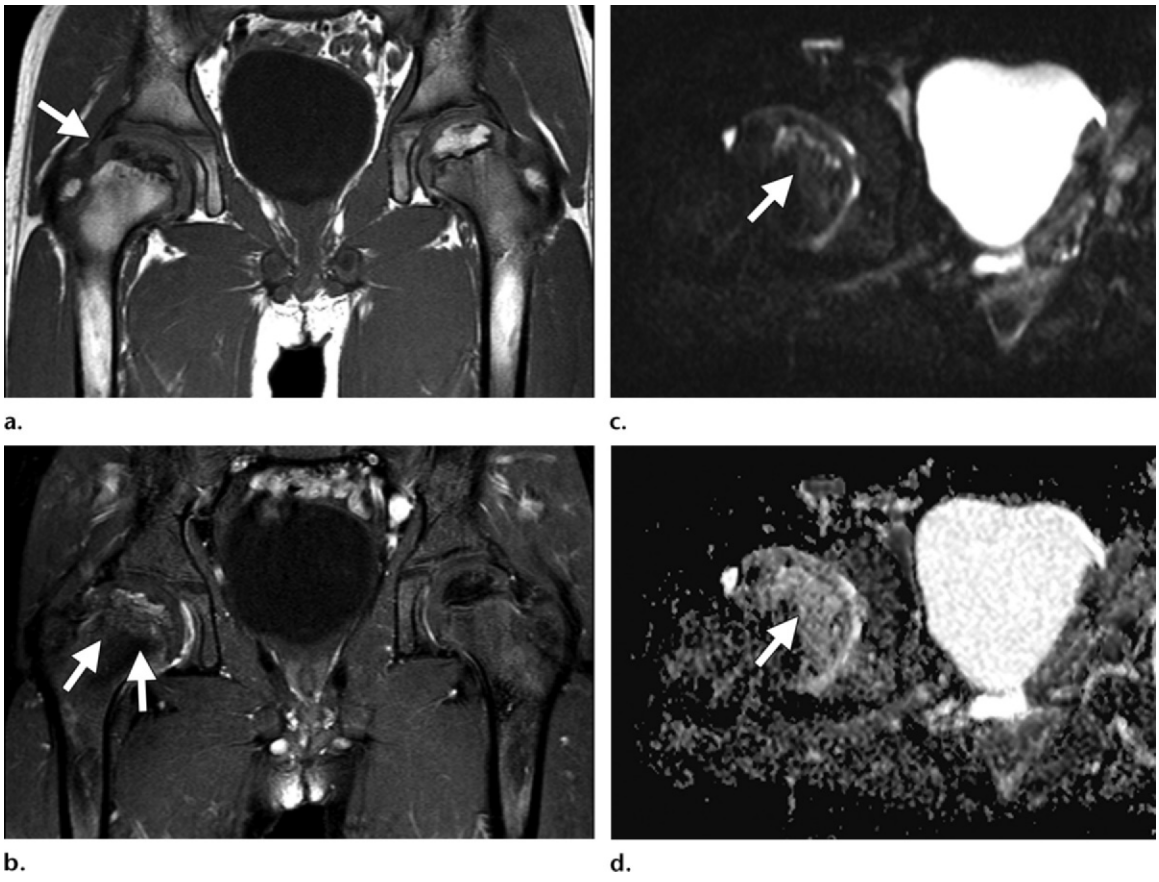

Figure 24. LCP disease in a 7-year-old boy with right hip pain. **(a)** Coronal T1-weighted MR image shows collapse of the right capital epiphysis, with central necrosis and lateral extrusion of the femoral head (arrow). Note the femoral notch on the left femoral head (a normal variant). **(b)** Coronal postcontrast T1-weighted MR image shows increased perfusion surrounding the region of necrosis (arrows). **(c, d)** Sagittal oblique diffusion-weighted **(c)** and ADC **(d)** images show increased diffusion in the anterior aspect of the proximal right femoral metaphysis (arrow).

locations include the proximal tibia, distal femur, proximal humerus, and proximal femur (73). The bones in the feet also are affected. Chondroblastomas usually manifest during the second and third decades of life and are twice as common in men as in women (74). Clinical symptoms include pain, usually of high severity; limitation of the adjacent joint; local tenderness; and swelling (72,73).

On MR images, chondroblastomas are seen as epiphyseal lesions with high T2 signal intensity surrounded by a halo of edema in the adjacent marrow and soft tissues (72). A characteristic thin (<1 mm) low-signal-intensity ring that corresponds to peripheral sclerosis is seen in more than 90% of lesions (Fig 25) (72,75). Fluid-fluid levels similar to those observed in aneurysmal bone cysts are seen in 20%–30% of chondroblastomas (75). Differential considerations include epiphyseal osteomyelitis and osteoid osteoma.

Other Tumoral Lesions.—Metastasis from a neuroblastoma can affect the epiphysis. Although the spine is the most common site of metastasis, metastasis from a neuroblastoma should be considered in the differential diagnosis of epiphyseal lesions in infants and children younger than 3 years. On T1-weighted MR images, skeletal metastases appear as patchy areas of low signal intensity because of the replacement of fatty marrow by tumor. Heterogeneous enhancement with intravenous contrast material and high signal intensity on fluid-sensitive MR images are also seen with metastatic disease (76). Hematologic malignancies such as leukemia or lymphoma typically manifest with diffuse invasion of the marrow. The infiltrative process replaces the fatty marrow and results in very low signal intensity on T1-weighted images and high signal intensity on fluid-sensitive MR images (77). Because of the diffuse nature of the disease, the signal intensity of the marrow tends to be homogeneous and can be misleading (Fig 26). Langerhan cell histiocytosis can also affect the epiphysis. Diagnosis is challenging because its imaging appearance is highly variable. Lesions usually have low signal intensity on T1-weighted images and high signal intensity on fluid-sensitive

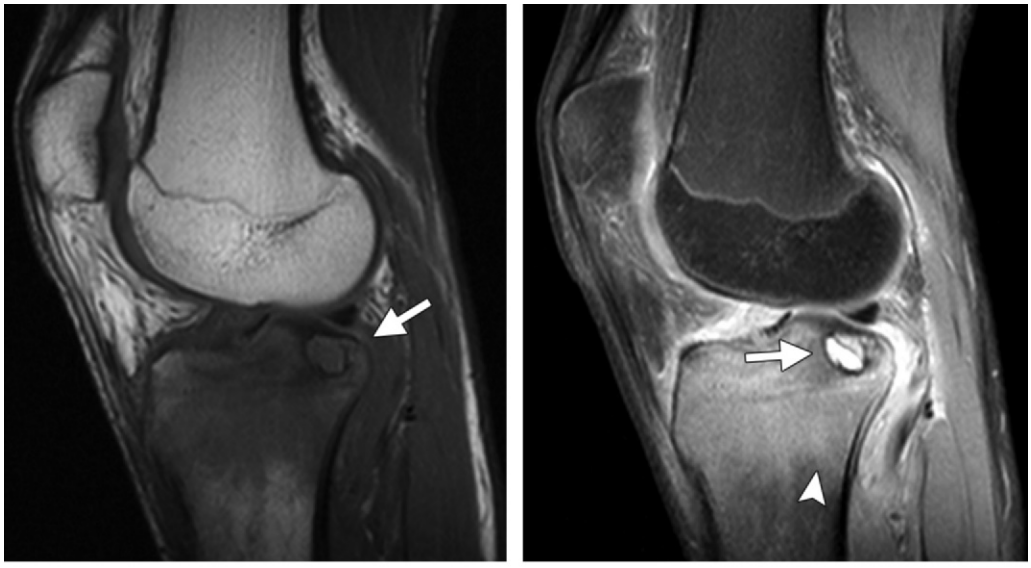

a. b.

Figure 25. Chondroblastoma in a 14-year-old male adolescent with knee pain. **(a)** Sagittal T1-weighted MR image of the knee shows a low-signal-intensity lesion in the proximal tibial epiphysis that is surrounded by a sclerotic rim of very low signal intensity (arrow) **(b)** Sagittal T2-weighted MR image demonstrates a well-defined rounded lesion surrounded by abundant marrow edema (arrowhead). An area of high signal intensity in the core of the lesion corresponds to the chondroid matrix (arrow).

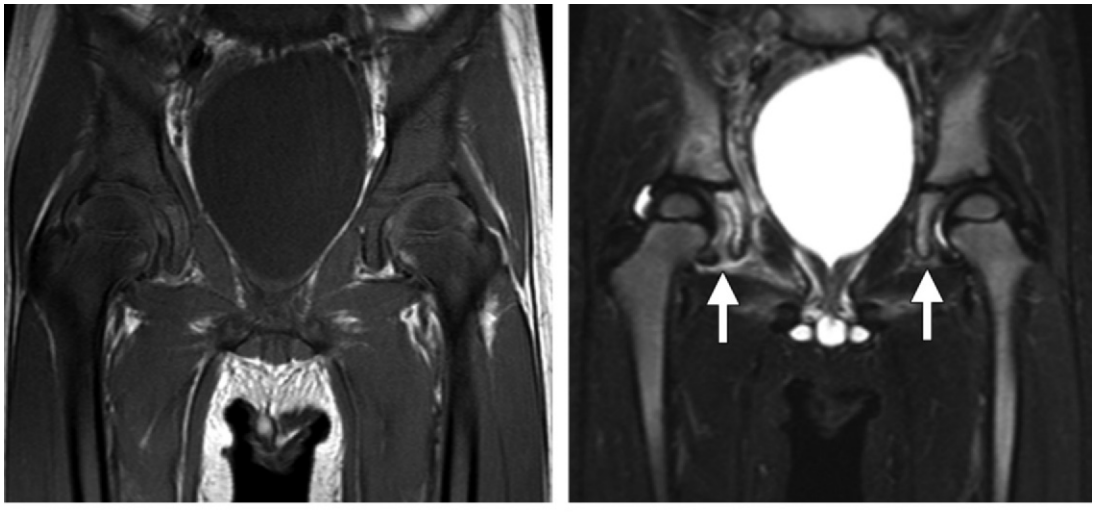

a. b.

Figure 26. MR imaging findings in a 3-year-old boy with fever, right leg pain, and newly diagnosed leukemia. **(a)** Coronal T1-weighted image of the pelvis demonstrates diffuse low signal intensity throughout the marrow and loss of the expected normal-appearing fatty epiphyses. **(b)** Coronal fluid-sensitive MR image demonstrates diffuse increased signal intensity in both epiphyses, which are isointense with the metaphyseal marrow, findings consistent with diffuse marrow leukemic infiltration. More focal signal intensity abnormality and soft-tissue edema are seen in the acetabular regions (right greater than left) (arrows), findings that represent bone infarcts.

images and are surrounded by edema. Diagnosis often requires tissue sampling (78).

Conclusion

Epiphyseal disorders are an important cause of morbidity in children. Many of these conditions, such as LCP disease and physeal fractures, are unique to the developing skeleton, and their manifestation varies with the degree of skeletal maturation. Injury to the SOC and physis can lead to early joint degeneration and growth arrest. MR imaging helps to accurately characterize various types of epiphyseal disorders, identify early complications, and guide treatment.

References

1. Laor T, Jaramillo D. MR imaging insights into skeletal maturation: what is normal? Radiology 2009;250(1):28–38.
2. Jaramillo D, Connolly SA, Mulkern RV, Shapiro F. Developing epiphysis: MR imaging characteristics and histologic correlation in the newborn lamb. Radiology 1998;207(3):637–645.
3. Jaramillo D, Villegas-Medina OL, Doty DK, et al. Age-related vascular changes in the epiphysis, physis, and metaphysis: normal findings on gadolinium-enhanced MRI of piglets. AJR Am J Roentgenol 2004;182(2):353–360.
4. Blumer MJ, Longato S, Fritsch H. Structure, formation and role of cartilage canals in the developing bone. Ann Anat 2008;190(4):305–315.
5. Borthakur A, Reddy R. Imaging cartilage physiology. Top Magn Reson Imaging 2010;21(5):291–296.
6. Raya JG, Arnoldi AP, Weber DL, et al. Ultra-high field diffusion tensor imaging of articular cartilage correlated with histology and scanning electron microscopy. MAGMA 2011;24(4):247–258.
7. Byers S, Moore AJ, Byard RW, Fazzalari NL. Quantitative histomorphometric analysis of the human growth plate from birth to adolescence. Bone 2000;27(4):495–501.
8. Ecklund K, Jaramillo D. Imaging of growth disturbance in children. Radiol Clin North Am 2001;39(4):823–841.
9. Laor T, Hartman AL, Jaramillo D. Local physeal widening on MR imaging: an incidental finding suggesting prior metaphyseal insult. Pediatr Radiol 1997;27(8):654–662.
10. Jaramillo D. Infection: musculoskeletal. Pediatr Radiol 2011;41(suppl 1):S127–S134.
11. Shapiro F, Connolly S, Zurakowski D, et al. Femoral head deformation and repair following induction of ischemic necrosis: a histologic and magnetic resonance imaging study in the piglet. J Bone Joint Surg Am 2009;91(12):2903–2914.
12. Jaramillo D, Laor T. Pediatric musculoskeletal MRI: basic principles to optimize success. Pediatr Radiol 2008;38(4):379–391.
13. Jaimes C, Jimenez M, Marin D, Ho-Fung V, Jaramillo D. The trochlear pre-ossification center: a normal developmental stage and potential pitfall on MR images. Pediatr Radiol 2012;42(11):1364–1371.
14. Jans LB, Jaremko JL, Ditchfield M, Verstraete KL. Evolution of femoral condylar ossification at MR imaging: frequency and patient age distribution. Radiology 2011;258(3):880–888.
15. Dwek JR, Shapiro F, Laor T, Barnewolt CE, Jaramillo D. Normal gadolinium-enhanced MR images of the developing appendicular skeleton. II. Epiphyseal and metaphyseal marrow. AJR Am J Roentgenol 1997;169(1):191–196.
16. Mirowitz SA. Hematopoietic bone marrow within the proximal humeral epiphysis in normal adults: investigation with MR imaging. Radiology 1993;188(3):689–693.
17. Shabshin N, Schweitzer ME, Morrison WB, Carrino JA, Keller MS, Grissom LE. High-signal T2 changes of the bone marrow of the foot and ankle in children: red marrow or traumatic changes? Pediatr Radiol 2006;36(7):670–676.
18. Burstein D, Velyvis J, Scott KT, et al. Protocol issues for delayed Gd (DTPA)(2-)-enhanced MRI (dGEMRIC) for clinical evaluation of articular cartilage. Magn Reson Med 2001;45(1):36–41.
19. Clinical practice guideline: early detection of developmental dysplasia of the hip—Committee on Quality Improvement, Subcommittee on Developmental Dysplasia of the Hip, American Academy of Pediatrics. Pediatrics 2000;105(1):896–905.
20. Shipman SA, Helfand M, Moyer VA, Yawn BP. Screening for developmental dysplasia of the hip: a systematic literature review for the US Preventive Services Task Force. Pediatrics 2006;117(3):e557–e576.
21. Jaramillo D, Villegas-Medina O, Laor T, Shapiro F, Millis MB. Gadolinium-enhanced MR imaging of pediatric patients after reduction of dysplastic hips: assessment of femoral head position, factors impeding reduction, and femoral head ischemia. AJR Am J Roentgenol 1998;170(6):1633–1637.
22. Barnewolt CE, Shapiro F, Jaramillo D. Normal gadolinium-enhanced MR images of the developing appendicular skeleton. I. Cartilaginous epiphysis and physis. AJR Am J Roentgenol 1997;169(1):183–189.
23. Tiderius C, Jaramillo D, Connolly S, et al. Post-closed reduction perfusion magnetic resonance imaging as a predictor of avascular necrosis in developmental hip dysplasia: a preliminary report. J Pediatr Orthop 2009;29(1):14–20.
24. Foad SL, Mehlman CT, Ying J. The epidemiology of neonatal brachial plexus palsy in the United States. J Bone Joint Surg Am 2008;90(6):1258–1264.
25. Hogendoorn S, van Overvest KL, Watt I, Duijsens AH, Nelissen RG. Structural changes in muscle and glenohumeral joint deformity in neonatal brachial plexus palsy. J Bone Joint Surg Am 2010;92(4):935–942.
26. Ruchelsman DE, Grossman JA, Price AE. Glenohumeral deformity in children with brachial plexus birth injuries. Bull NYU Hosp Jt Dis 2011;69(1):36–43.
27. Waters PM, Smith GR, Jaramillo D. Glenohumeral deformity secondary to brachial plexus birth palsy. J Bone Joint Surg Am 1998;80(5):668–677.
28. Sabharwal S. Blount disease. J Bone Joint Surg Am 2009;91(7):1758–1776.
29. Pirpiris M, Jackson KR, Farng E, Bowen RE, Otsuka NY. Body mass index and Blount disease. J Pediatr Orthop 2006;26(5):659–663.
30. Sabharwal S, Wenokor C, Mehta A, Zhao C. Intra-articular morphology of the knee joint in children with Blount disease: a case-control study using MRI. J Bone Joint Surg Am 2012;94(10):883–890.
31. Murphey MD, Choi JJ, Kransdorf MJ, Flemming DJ, Gannon FH. Imaging of osteochondroma: variants and complications with radiologic-pathologic correlation. RadioGraphics 2000;20(5):1407–1434.
32. Rosero VM, Kiss S, Terebessy T, Köllö K, Szöke G. Dysplasia epiphysealis hemimelica (Trevor's disease): 7 of our own cases and a review of the literature. Acta Orthop 2007;78(6):856–861.
33. Azouz EM, Slomic AM, Marton D, Rigault P, Finidori G. The variable manifestations of dysplasia epiphysealis hemimelica. Pediatr Radiol 1985;15(1):44–49.
34. Borges JL, Guille JT, Bowen JR. Köhler's bone disease of the tarsal navicular. J Pediatr Orthop 1995;15(5):596–598.
35. Rosenberg ZS, Beltran J, Bencardino JT. MR imaging of the ankle and foot. RadioGraphics 2000;20(Spec No):S153–S179.
36. Kan JH, Kleinman PK. Pediatric and adolescent musculoskeletal MRI: a case-based approach. New York, NY: Springer, 2007.
37. Mann DC, Rajmaira S. Distribution of physeal and nonphyseal fractures in 2,650 long-bone fractures in children aged 0-16 years. J Pediatr Orthop 1990;10(6):713–716.
38. Peterson HA, Madhok R, Benson JT, Ilstrup DM, Melton LJ 3rd. Physeal fractures. I. Epidemiology in Olmsted County, Minnesota, 1979-1988. J Pediatr Orthop 1994;14(4):423–430.
39. Smith BG, Rand F, Jaramillo D, Shapiro F. Early MR imaging of lower-extremity physeal fracture-separations: a preliminary report. J Pediatr Orthop 1994;14(4):526–533.

40. Khoshhal KI, Kiefer GN. Physeal bridge resection. J Am Acad Orthop Surg 2005;13(1):47–58.
41. Laor T, Wall EJ, Vu LP. Physeal widening in the knee due to stress injury in child athletes. AJR Am J Roentgenol 2006;186(5):1260–1264.
42. Jaimes C, Jimenez M, Shabshin N, Laor T, Jaramillo D. Taking the stress out of evaluating stress injuries in children. RadioGraphics 2012;32(2):537–555.
43. Dwek JR, Cardoso F, Chung CB. MR imaging of overuse injuries in the skeletally immature gymnast: spectrum of soft-tissue and osseous lesions in the hand and wrist. Pediatr Radiol 2009;39(12):1310–1316.
44. Oeppen RS, Connolly SA, Bencardino JT, Jaramillo D. Acute injury of the articular cartilage and subchondral bone: a common but unrecognized lesion in the immature knee. AJR Am J Roentgenol 2004;182(1):111–117.
45. Zaidi A, Babyn P, Astori I, White L, Doria A, Cole W. MRI of traumatic patellar dislocation in children. Pediatr Radiol 2006;36(11):1163–1170.
46. Potter HG, Linklater JM, Allen AA, Hannafin JA, Haas SB. Magnetic resonance imaging of articular cartilage in the knee: an evaluation with use of fast-spin-echo imaging. J Bone Joint Surg Am 1998;80(9):1276–1284.
47. Laor T, Zbojniewicz AM, Eismann EA, Wall EJ. Juvenile osteochondritis dissecans: is it a growth disturbance of the secondary physis of the epiphysis? AJR Am J Roentgenol 2012;199(5):1121–1128.
48. Hefti F, Beguiristain J, Krauspe R, et al. Osteochondritis dissecans: a multicenter study of the European Pediatric Orthopedic Society. J Pediatr Orthop B 1999;8(4):231–245.
49. Wall E, Von Stein D. Juvenile osteochondritis dissecans. Orthop Clin North Am 2003;34(3):341–353.
50. De Smet AA, Fisher DR, Graf BK, Lange RH. Osteochondritis dissecans of the knee: value of MR imaging in determining lesion stability and the presence of articular cartilage defects. AJR Am J Roentgenol 1990;155(3):549–553.
51. Kijowski R, Blankenbaker DG, Shinki K, Fine JP, Graf BK, De Smet AA. Juvenile versus adult osteochondritis dissecans of the knee: appropriate MR imaging criteria for instability. Radiology 2008;248(2):571–578.
52. Guillerman RP. Osteomyelitis and beyond. Pediatr Radiol 2013;43(suppl 1):S193–S203.
53. Browne LP, Guillerman RP, Orth RC, Patel J, Mason EO, Kaplan SL. Community-acquired staphylococcal musculoskeletal infection in infants and young children: necessity of contrast-enhanced MRI for the diagnosis of growth cartilage involvement. AJR Am J Roentgenol 2012;198(1):194–199.
54. Saisu T, Kawashima A, Kamegaya M, Mikasa M, Morishi J, Moriya H. Humeral shortening and inferior subluxation as sequelae of septic arthritis of the shoulder in neonates and infants. J Bone Joint Surg Am 2007;89(8):1784–1793.
55. Kwack KS, Cho JH, Lee JH, Cho JH, Oh KK, Kim SY. Septic arthritis versus transient synovitis of the hip: gadolinium-enhanced MRI finding of decreased perfusion at the femoral epiphysis. AJR Am J Roentgenol 2007;189(2):437–445.
56. Forlin E, Milani C. Sequelae of septic arthritis of the hip in children: a new classification and a review of 41 hips. J Pediatr Orthop 2008;28(5):524–528.
57. Lejman T, Strong M, Michno P, Hayman M. Septic arthritis of the shoulder during the first 18 months of life. J Pediatr Orthop 1995;15(2):172–175.
58. Lavernia CJ, Sierra RJ, Grieco FR. Osteonecrosis of the femoral head. J Am Acad Orthop Surg 1999;7(4):250–261.
59. Rao VM, Mitchell DG, Steiner RM, et al. Femoral head avascular necrosis in sickle cell anemia: MR characteristics. Magn Reson Imaging 1988;6(6):661–667.
60. Zibis AH, Karantanas AH, Roidis NT, et al. The role of MR imaging in staging femoral head osteonecrosis. Eur J Radiol 2007;63(1):3–9.
61. Malizos KN, Karantanas AH, Varitimidis SE, Dailiana ZH, Bargiotas K, Maris T. Osteonecrosis of the femoral head: etiology, imaging and treatment. Eur J Radiol 2007;63(1):16–28.
62. Yousefzadeh DK, Jaramillo D, Johnson N, Doerger K, Sullivan C. Biphasic threat to femoral head perfusion in abduction: arterial hypoperfusion and venous congestion. Pediatr Radiol 2010;40(9):1517–1525.
63. Kim HK. Legg-Calvé-Perthes disease. J Am Acad Orthop Surg 2010;18(11):676–686.
64. Mitchell DG, Kressel HY, Arger PH, Dalinka M, Spritzer CE, Steinberg ME. Avascular necrosis of the femoral head: morphologic assessment by MR imaging, with CT correlation. Radiology 1986;161(3):739–742.
65. Jain R, Sawhney S, Rizvi SG. Acute bone crises in sickle cell disease: the T1 fat-saturated sequence in differentiation of acute bone infarcts from acute osteomyelitis. Clin Radiol 2008;63(1):59–70.
66. Lamer S, Dorgeret S, Khairouni A, et al. Femoral head vascularisation in Legg-Calvé-Perthes disease: comparison of dynamic gadolinium-enhanced subtraction MRI with bone scintigraphy. Pediatr Radiol 2002;32(8):580–585.
67. MacKenzie JD, Gonzalez L, Hernandez A, Ruppert K, Jaramillo D. Diffusion-weighted and diffusion tensor imaging for pediatric musculoskeletal disorders. Pediatr Radiol 2007;37(8):781–788.
68. de Sanctis N, Rega AN, Rondinella F. Prognostic evaluation of Legg-Calvé-Perthes disease by MRI. I. The role of physeal involvement. J Pediatr Orthop 2000;20(4):455–462.
69. Jaramillo D, Kasser JR, Villegas-Medina OL, Gaary E, Zurakowski D. Cartilaginous abnormalities and growth disturbances in Legg-Calvé-Perthes disease: evaluation with MR imaging. Radiology 1995;197(3):767–773.
70. Ha AS, Wells L, Jaramillo D. Importance of sagittal MR imaging in nontraumatic femoral head osteonecrosis in children. Pediatr Radiol 2008;38(11):1195–1200.
71. Yoo WJ, Kim YJ, Menezes NM, Cheon JE, Jaramillo D. Diffusion-weighted MRI reveals epiphyseal and metaphyseal abnormalities in Legg-Calvé-Perthes disease: a pilot study. Clin Orthop Relat Res 2011;469(10):2881–2888.
72. Oxtoby JW, Davies AM. MRI characteristics of chondroblastoma. Clin Radiol 1996;51(1):22–26.
73. Dahlin DC, Ivins JC. Benign chondroblastoma: a study of 125 cases. Cancer 1972;30(2):401–413.
74. Jee WH, Park YK, McCauley TR, et al. Chondroblastoma: MR characteristics with pathologic correlation. J Comput Assist Tomogr 1999;23(5):721–726.
75. Kaim AH, Hügli R, Bonél HM, Jundt G. Chondroblastoma and clear cell chondrosarcoma: radiological and MRI characteristics with histopathological correlation. Skeletal Radiol 2002;31(2):88–95.
76. Meyer JS, Siegel MJ, Farooqui SO, Jaramillo D, Fletcher BD, Hoffer FA. Which MRI sequence of the spine best reveals bone-marrow metastases of neuroblastoma? Pediatr Radiol 2005;35(8):778–785.
77. Ruzal-Shapiro C, Berdon WE, Cohen MD, Abramson SJ. MR imaging of diffuse bone marrow replacement in pediatric patients with cancer. Radiology 1991;181(2):587–589.
78. Beltran J, Aparisi F, Bonmati LM, Rosenberg ZS, Present D, Steiner GC. Eosinophilic granuloma: MRI manifestations. Skeletal Radiol 1993;22(3):157–161.

RadioGraphics

MR Imaging of Normal Epiphyseal Development and Common Epiphyseal Disorders

Camilo Jaimes, MD • Nancy A. Chauvin, MD • Jorge Delgado, MD • Diego Jaramillo, MD, MPH

RadioGraphics 2014; 34:449–471 • **Published online** 10.1148/rg.342135070 • **Content Codes:** MK MR PD

Page 451
During infancy, normal transphyseal vessels serve as anastomoses between the epiphyseal and metaphyseal vascular beds. Fenestrations on the physis increase the epiphyseal vascular supply but allow pathologic conditions such as infection to spread. Transphyseal anastomoses decrease with age and completely disappear at approximately 18 months of age.

Page 455
The outermost region of the SOC is richly vascularized, contains hematopoietic marrow, and is a site of endochondral ossification. Physiologically, this region is equivalent to a metaphysis and responds similarly to insults.

Page 460
Horizontal fractures (Salter-Harris types I and II) result in bridge formation in 25% of cases, whereas longitudinal fractures (Salter-Harris types III and IV) result in bridge formation in 75% of cases. The specific physis affected by the fracture, however, is the main determinant of the subsequent risk of growth arrest.

Page 465
Involvement of the epiphyseal cartilage with abscess formation and destruction of the physis manifests as enhancement defects on postcontrast images. These findings carry a poor prognosis with increased risk of growth arrest. Furthermore, findings at unenhanced T1-weighted or fluid-sensitive MR imaging can appear normal.

Page 467
Prognostic indicators in LCP disease include age of onset, extent of femoral head deformity and fragmentation, lateral extrusion, physeal involvement, and metaphyseal abnormalities. Metaphyseal cysts and physeal abnormalities are believed to be predictors of poor outcome.